Critical functions and key interactions mediated by the RNase E scaffolding domain in *Pseudomonas aeruginosa*

Sandra Amandine Marie Geslain, Stéphane Hausmann, Johan Geiser, George Edward Allen, Diego Gonzalez and Martina Valentini*

Department of Microbiology and Molecular Medicine, CMU, Faculty of Medicine, University of Geneva, Geneva, Switzerland.

* To whom correspondence should be addressed. e-mail: Martina.Valentini@unige.ch

Abstract

The RNA degradosome is a bacterial multi-protein complex mediating mRNA processing and degradation. In Pseudomonadota, this complex assembles on the C-terminal domain (CTD) of RNase E through short linear motifs (SLiMs) that determine its composition and functionality. In the human pathogen *Pseudomonas aeruginosa*, the RNase E CTD exhibits limited similarity to that of model organisms, impeding our understanding of RNA metabolic processes in this bacterium. Our study systematically maps the interactions mediated by the *P. aeruginosa* RNase E CTD and highlights its critical role in transcript regulation and cellular functions. We identified the SLiMs crucial for membrane attachment, RNA binding and complex clustering, as well as for direct binding to the core components PNPase and RhlB. Transcriptome analyses of RNase E CTD mutants revealed altered expression of genes involved in quorum sensing, type III secretion, and amino acid metabolism. Additionally, we show that the mutants are impaired in cold adaptation, pH response, and virulence in an infection model. Overall, this work establishes the essential role of the RNA degradosome in driving bacterial adaptability and pathogenicity.

Author summary

Bacteria must rapidly adapt to changing environments, whether facing temperature shifts, nutrient scarcity, or antibiotic exposure. A key mechanism enabling this adaptability is the regulation of mRNA levels—the molecular blueprints for protein production. This process is governed by the RNA degradosome, a multi-protein complex that processes and degrades RNA to control gene expression. Although the RNA degradosome core function is conserved across bacteria, its composition and organization differ significantly between species, reflecting diverse lifestyles and environmental challenges each bacterium encounter.

In this study, we investigated the RNA degradosome in *Pseudomonas aeruginosa*, a bacterial pathogen causing difficult-to-treat infections in humans. We identified its components and mapped regions within the complex essential for RNA binding, membrane attachment, and spatial organization. Disrupting these regions compromised *P. aeruginosa* ability to survive in cold conditions, respond to stress, and establish an infection. Through this work, we uncovered unique features of the *P. aeruginosa* RNA degradosome that distinguish it from those of other species, emphasizing the RNA degradosome critical role in bacterial adaptability and highlight it as a promising target for therapies against *P. aeruginosa* infections.

45 **Introduction**

46 In bacteria, the processing and degradation of mRNAs is primarily orchestrated by the RNA
47 degradosome, a multi-enzyme complex that includes ribonucleases, RNA helicases, and various other
48 proteins [1-5]. The RNA degradosome plays a crucial role in enabling bacteria to rapidly adapt to
49 changing environmental conditions by swiftly modifying mRNA levels and broadly regulating gene
50 expression [6, 7].

51 Most of our knowledge on the RNA degradosome derives from studies in *Escherichia coli*, where the
52 RNase E endonuclease serves as the central component [8-11]. While the catalytic activity of *E. coli*
53 RNase E resides in its N-terminal domain (NTD, amino acids 1-529), the C-terminal domain (CTD,
54 amino acids 530-1061), or scaffolding domain, is intrinsically disordered and contains short linear
55 motifs (SLiMs) of 10 to 40 amino acids to which the other RNA degradosome components bind [11,
56 12]. Core *E. coli* RNA degradosome components, namely the polyribonucleotide phosphorylase
57 PNPase [13], the RNA helicase RhlB [14], and the glycolytic enzyme enolase [15], interact with RNase
58 E in semi-stoichiometric ratios via the PBS (PNPase binding site), HBS (helicase binding site) and EBS
59 (enolase binding cite) SLiM, respectively [16, 17]. The *E. coli* RNase E CTD also includes an
60 amphipathic helix, called membrane targeting sequence (MTS), which tethers the entire complex to the
61 inner membrane, and at least two RNA-binding SLiMs, AR1 (named also RBD) and AR2, which
62 mediate contact with translating ribosomes, small non-coding RNAs and mRNAs [12, 18-21].
63 Additional proteins, such as RraA [22, 23], RraB [24], CsdA [25], Ppk [26], MinD [27, 28], and Hfq
64 [29], can interact with *E. coli* RNase E in sub-stochiometric ratios and/or under non-standard conditions
65 of growth (reviewed in [30]). Of importance, the RNase E NTD is essential for *E. coli* growth and rRNA
66 processing [31], whereas deletion of the CTD is not lethal and alters mRNA levels without affecting
67 rRNAs [19, 32-34]. This highlights the dual role of RNase E, with the NTD being crucial for overall
68 cell maintenance, and the CTD regulating specific RNA substrates through the assembly of the RNA
69 degradosome.

70 RNase E orthologs are present in approximately 49% of sequenced bacterial genomes, and nearly all
71 Pseudomonadota (formerly called Proteobacteria) encode at least one RNase E ortholog, with the
72 notable exception of most *Campylobacter* and *Helicobacter* species [5, 30]. The RNase E NTD is

remarkably conserved across most species, while the CTD varies considerably in sequence, length, and SLiMs composition, even between species belonging to the same order [30]. SLiMs variability is thought to drive the diversity of RNase E interacting partners, and therefore RNA degradosome composition, among bacterial species. For instance, in *Caulobacter crescentus,* RNase E interacts with PNPase, RhlB, RNase D, and the Krebs cycle enzyme aconitase [35, 36]. In *Anabaena* sp. strain PCC 7120, RNase E partners with PNPase, enolase, the RNA helicase CrhB, and RNase II [37-39], while in *Pseudomonas syringae* LZ4W, only RNase R and the RNA helicase RhlE were found to co-purify with RNase E in pull-down assays [40]. Similarly, in *Rhodobacter capsulatus*, purification of the RNA degradosome complex via glycerol-gradient centrifugation of cell extracts revealed the presence of RNase E, two unnamed RNA helicases, the Rho transcription termination factor, and two unidentified proteins of 47 and 36 kDa, with only low amounts of PNPase present in the purified fractions [41].

In these examples, the SLiMs mediating protein-protein interactions were not always characterized. Moreover, even when the interaction of RNase E with a certain protein partner is conserved across several species, such as the RNase E-PNPase and RNase E-RhlB interactions, the SLiMs involved in the binding show little sequence identity [30, 36, 37, 42-44]. Therefore, predicting RNA degradosome composition based solely on the RNase E CTD sequence does not seem possible. Experimental characterization of the SLIMs across different bacterial species and their impact on the RNA degradosome composition and function is essential, providing insights into novel regulatory mechanisms that enable bacteria to thrive under stress and adapt to diverse environments.

Little is known about the RNA degradosome composition of the opportunistic human pathogen *Pseudomonas aeruginosa*, which is a leading cause of nosocomial infections worldwide largely due to its remarkable adaptability to different environments and resistance to antibiotics [45-53]. A recent study has revealed that *P. aeruginosa* RNase E co-elutes with PNPase, the PA0428 RNA helicase, and several other proteins in pull-down assays, although their interaction with RNase E has neither been confirmed nor mapped [54]. Our laboratory has characterized the PA0428 RNA helicase, named RhlE2, confirming an RNA-dependent interaction with RNase E and identifying the RhlE2 C-terminal region as necessary and sufficient for this binding [55, 56]. However, the specific RNase E interaction site remained unmapped.

101 In this study, we characterize the SLiMs within the CTD of *P. aeruginosa* RNase E, identifying those
102 involved in RNA binding (AR1, AR4, and REER-repeats) as well as those mediating interactions with
103 core RNA degradosome components, which we determine to be PNPase and the RNA helicase RhlB
104 (NDPR and AR1, respectively). We also show that RhlE2 interacts with the RNase E NTD in pull-down
105 assays. Protein-protein interactions were probed with multiple experimental approaches, including an
106 analysis of the subcellular localization dynamics of the complex. Additionally, we performed
107 transcriptomic and phenotypic analyses of RNase E CTD mutant strains, revealing the critical role of
108 RNA degradosome complex scaffolding in bacterial virulence, adaptation to cold temperatures and to
109 pH fluctuations.
110 The ability of *P. aeruginosa* to cause disease is intrinsically linked to a sophisticated gene regulatory
111 network that facilitates bacterial survival and virulence. Within this network, the role of post-
112 transcriptional gene regulation remains only partially explored [57, 58]. By uncovering the composition
113 and functional dynamics of the RNA degradosome in *P. aeruginosa*, our study not only advances the
114 understanding of the molecular mechanisms driving bacterial environmental adaptation but also reveals
115 potential novel drug targets, which could be crucial in the fight against antibiotic-resistant infections.
116

117 **Results**

118 **The P. *aeruginosa* RNase E harbours several uncharacterised SLiMs conserved within the**
119 **Pseudomonadales**

120 *P. aeruginosa* RNase E (Pa RNase E) consists of an NTD (amino acids 1-529) that shares high sequence
121 identity (70%) and similarity (90%) with the NTD of *E. coli* RNase E (Ec RNase E), and a CTD (amino
122 acids 530-1057) that shows only 25% identity and 37% similarity with the CTD of Ec RNase E (Fig.
123 S1). Previous work by Aït-Bara et al. (2015) identified seven different putative SLiMs on the Pa RNase
124 E CTD (MTS, AR4, REE, M29, AR1, M20 and NDPR) [30], which are shown in comparison to the Ec
125 RNase E in Fig. S2A. Of note, the MTS is the only SLiM of Pa RNase E CTD with a propensity to form
126 a secondary structure while in Ec RNase E, the helicase, enolase, and PNPase binding sites also exhibit
127 this feature (Fig. 1 and [12]).

128 To refine the prediction of Pa RNase E SLiMs, we performed a multiple sequence alignment of 5000
129 *Pseudomonas* RNase E orthologs, identifying conserved motifs (Fig. S3). Several highly conserved
130 CTD regions overlap with the SLiMs previously identified, with the notable presence of additional
131 conserved residues located immediately adjacent to these SLiMs (Fig. S2A, Fig. S3). Based on these
132 data, we updated the SLiMs boundaries to include these conserved residues (Fig. 1B, former SLiMs
133 boundaries in Fig. S2A). Upon manual inspection of the CTD sequence, we also observed a large
134 duplicated sequence (residues 635-667 and 682-714) within the CTD region containing the REE and
135 motif 29 SLiMs. Since motif 29 is defined by the conserved motif REERQPR, we merged the two
136 SLiMs and renamed the entire segment (residues 614-729) as the "REER-repeats" region (Fig. 1B). The
137 number of REER repeats varies across *Pseudomonas* species: *P. aeruginosa* strains typically harbour
138 13 RE[ED]R repeats, whereas the *P. fluorescens*, *P. protegens*, *P. stutzeri*, and *P. syringae* environmental
139 species show a distribution of repeats peaking around 8-10. The exception is *P. putida*, which exhibits
140 a high frequency of 20-23 RE[ED]R repeats (Fig. S2B). This variability suggests a high frequency of
141 indels occurring within the REER-repeats region.
142 Overall, our in-silico analyses of Pa RNase E CTD sequence refined the number and length of the Pa
143 RNase E SLiMs, highlighting a potential functional significance of the REER-repeats region in
144 *Pseudomonas* species, and suggesting differences in RNA degradosome complex dynamics between *P.*
145 *aeruginosa* and *E. coli*.
146
147 **The REER-repeats, AR1 and AR4 SLiMs mediate RNase E CTD RNA binding and foci formation**
148 Previous works in *E. coli* identified arginine-rich SLiMs as RNA-binding motifs [21, 59]. We therefore
149 hypothesized that the *P. aeruginosa* AR1 and AR4 SLiMs, along with the newly identified REER-repeat
150 region, might be involved in RNA binding. To test this hypothesis, we conducted electrophoretic
151 mobility shift assays (EMSA) to examine the binding of purified RNase E CTD proteins to an *in vitro*
152 synthesized RNA derived from the *malEF* intergenic region (for details, see methods). We tested wild-
153 type (WT) CTD and mutated variants where arginine residues in AR1, AR4, or the REER-repeats were
154 replaced with alanine (named AR1mut, AR4mut, and REERmut, respectively; see Table S4 for a
155 description of the mutations). Qualitative analysis of the EMSA showed that the WT, AR1mut, and

156 AR4mut variants bound RNA with similar efficiency, as indicated by comparable gel shift patterns (Fig.
157 S4A, Fig. 2A). However, the REERmut variant exhibited slightly reduced RNA binding, evidenced by
158 a delayed shift as compared to the former proteins (Fig. S4B and 2A). The combination of AR1 and
159 AR4 mutations resulted in an impaired RNA binding which was further exacerbated when the REER
160 mutation was also introduced: no observable shift in the RNA was detected when incubated with the
161 protein variant carrying mutations in all three SLiMs, even at an RNA-to-protein ratio of 1:80 (Fig. 2A).
162 Together, these results highlight the functional redundancy of the AR1, AR4, and REER-repeat SLiMs
163 in RNA binding, as a complete defect in RNA binding is observed only when all these SLiMs are
164 simultaneously disrupted.
165 One notable characteristic of the RNA degradosome is its tendency to form highly dynamic subcellular
166 foci, also referred to as "clusters," "puncta," or "helical structures" [28, 60]. These foci rapidly
167 disassemble upon rifampicin treatment, suggesting their formation is RNA-dependent [60, 61]. In *E.*
168 *coli*, these foci are membrane-anchored via the MTS SLiM, whereas in *C. crescentus* they remain
169 cytoplasmic, driven by liquid-liquid phase separation [61, 62]. To investigate the subcellular localisation
170 of Pa RNase E, we constructed *P. aeruginosa* PAO1 strains expressing msfGFP-tagged Pa RNase E, Pa
171 RNase E^{1-588}, or Pa RNase E^{1-529} from the native *rne* locus. The two RNase E truncations were designed
172 based on our in-silico analysis of Pa RNase E SLiMs, assuming that they would lack the capacity to
173 assemble the RNA degradosome. The key difference between RNase E^{1-588} and RNase E^{1-529} lies in the
174 presence of the MTS (Fig. 1B). Visualization using epifluorescence microscopy revealed that RNase E-
175 msfGFP forms foci concentrated near the cell edge (Fig 2B). Both CTD truncation mutants showed
176 impairment in foci assembly, but while the RNase E^{1-588}-msfGFP protein localises uniformly around the
177 edge of the bacteria, the RNase E^{1-529}-msfGFP mutant protein additionally fails to localise near the
178 membrane, consistent with the role of the MTS in membrane anchoring (Fig. 2B-C).
179 Exposure of Pa RNase E-msfGFP expressing cells to high levels of rifampicin (100 µg/ml) led to the
180 dissipation of these foci, resulting in a smoother distribution of the signal along the cell periphery, which
181 phenocopies the localization of the RNase E^{1-588}-msfGFP strain (Fig. 2D). Quantitative analysis
182 confirmed a significant reduction in signal intensity variance upon rifampicin treatment as compared to

183 the control (DMSO-only), indicating foci dissipation, while the average signal intensity remained
184 constant, ruling out RNase E- msfGFP proteolysis (Fig. 2E-F, Fig. S4F).
185 To further verify that Pa RNase E-msfGFP foci formation depends on CTD-mediated RNA binding, we
186 constructed *P. aeruginosa* strains with chromosomally msfGFP-tagged RNase E variants mutated in
187 AR1, AR4, and REER-repeats SLiMs, individually and in combination, as described previously for the
188 EMSA. Visualisation of these variants showed a clear correlation between CTD-mediated RNA binding
189 and foci formation. Specifically, the RNase E AR1+AR4mut-msfGFP showed less distinct foci and
190 lower signal variance compared to RNase E-msfGFP and single AR1 or AR4 mutants (Fig. 2B-C). The
191 RNase E REERmut-msfGFP also had diffuse foci and lower variance, while the RNase E
192 AR1+AR4+REERmut-msfGFP, with abolished RNA binding, displayed the most severe disruption,
193 with nearly complete loss of foci and a very narrow signal intensity distribution (Fig. 2B-C and Fig.
194 S4F). Similar patterns were observed with four other CTD truncations containing different
195 combinations of RNA-binding SLiMs, ruling out the possibility that this foci dissipation is caused by
196 the changes in the charge of the CTD conferred by the Arg to Ala mutations (Fig. S4E).
197 Of note, we noticed an increased signal intensity in all the msfGFP-tagged RNase E mutants tested as
198 compared to the RNase E-msfGFP (Fig. S4C). Since all constructs are expressed at the native locus,
199 this could likely reflect higher RNase E protein levels, which suggests that CTD-mediated RNA binding
200 might be necessary for RNase E autoregulation [63]. To confirm this, we performed a Western Blot on
201 strains expressing several Strep-tagged RNase E mutants and could indeed observe that RNase E protein
202 levels are increased upon deletion of the CTD or introduction of AR1+AR4+REERmut (Fig. S4D).
203 Overall, we conclude that in *P. aeruginosa*, the organisation of the RNA degradosome complex into
204 visualisable foci is dependent on the RNase E CTD-mediated RNA binding and suggest that this
205 interaction not only organizes the localisation of the RNA degradosome but could also influence the
206 regulatory activity of RNase E.
207
208 **Identification of proteins binding to RNase E scaffold domain**
209 In *P. aeruginosa*, the RNA degradosome was proposed to include the RhlE2 RNA helicase (PA0428),
210 PNPase, and other associated proteins [54, 55]. However, the direct nature of these interactions and the

211 specific interaction sites have not been demonstrated nor mapped. Additionally, RNase R was also
212 suggested to be a *P. aeruginosa* RNA degradosome component, as it is in *P. syringae* LZ4W [30, 40].
213 To test these hypotheses and identify Pa RNase E CTD interacting proteins, we performed a pull-down
214 assay using *P. aeruginosa* strains expressing C-terminal Strep II-tagged full-length RNase E (RNase E^{1-}
215 ^{1057}-Strep) or an RNase E truncation missing the entire CTD (RNase E^{1-529}-Strep). As an additional
216 control, the assay was also performed with the *P. aeruginosa* PAO1 wild-type (WT) to discard proteins
217 interacting nonspecifically with the Strep-Tactin magnetic beads (Fig. 3A-B).
218 Eluates of the pull-down experiment were first analysed by silver staining (Fig S5A). The RNase E^{1-}
219 ^{1057}-Strep eluate revealed a high molecular weight band corresponding to RNase E, along with additional
220 bands absent in the untagged and RNase E^{1-529}-Strep samples. These bands likely represent components
221 of the RNA degradosome or cleaved RNase E^{1-1057}-Strep intermediates, as RNase E is known to be
222 prone to cleavage [42, 64]. Mass spectrometry (LC-MS/MS) analysis identified a total of 115 proteins
223 present in both duplicates of the RNase E^{1-1057}-Strep eluates. 13 proteins (including RNase E) were
224 enriched by at least 5.5-fold as compared with the untagged sample (Fig. 3A). This stringent threshold
225 was chosen since core components of the RNA degradosome should be abundantly associated to RNase
226 E. Of these 12 putative partners, 5 (PNPase, GdhB, ArcB, RhlB and RpoB) were completely absent
227 from both RNase E^{1-529}-Strep duplicates and 2, namely RpoC and RplL, were absent from one replicate
228 and present in the second replicate with a peptide count of 2 (Fig. 3B). We selected for further study the
229 first 5 proteins, which were considered the most promising RNA degradosome candidates as their
230 interaction with Pa RNase E seemed fully dependent on the CTD.
231 It is worth noting that the RhlE2 RNA helicase was, as expected [54, 55], among the proteins enriched
232 in the RNase E^{1-1057}-Strep eluate as compared to the untagged control, but surprisingly it was equally
233 enriched in the RNase E^{1-529}-Strep eluate condition (Fig 3B), indicating that this interaction occurs via
234 RNase E NTD and not via the CTD.
235
236 **RNase E direct interaction with PNPase and RhlB occurs via the NDPR and AR1 SLiMs,**
237 **respectively**

238 The interaction between RNase E and the 5 candidates was first verified using an adenylate-cyclase-
239 based bacterial two-hybrid (BTH) assay [65]. Co-expression of T25-PNPase and T25-RhlB with T18-
240 RNase E resulted in red colonies on MacConkey agar and a significant increase of β-galactosidase
241 activity compared to empty vector controls (11-fold or 5-fold increase, respectively), confirming their
242 interaction (Fig. S6A, Fig. 3C). Co-expression of T25-ArcB with T18-RNase E also resulted in a
243 significant increase in β-galactosidase activity (5-fold increase) compared to the negative control (Fig.
244 3C, Fig. S6A). To identify the SLiMs mediating the observed interactions, we generated seven CTD
245 truncations of RNase E, each lacking an additional SLiM as compared with the longer version. Testing
246 these truncations for their capacity to interact with PNPase revealed that only T18-RNase E^{1-1025} showed
247 β-galactosidase activity similar to those of T18-RNase E^{1-1057} upon co-expression with T25-PNPase
248 (Fig. 3D, Fig. S6B). In contrast, all shorter T18-RNase E CTD truncations except T18-RNase E^{1-529},
249 and also T18-RNase $E^{940-1057}$, exhibited a significant increase of β-galactosidase activity as compared
250 with the negative controls but lower than T18-RNase E^{1-1057} (Fig. 3D, Fig. S6B). Overall, this suggests
251 that PNPase interaction with RNase E relies on a complex binding site involving RNase E residues 529-
252 588 and 940-1057.
253 Co-expression of the T18-RNase E CTD truncations with T25-RhlB revealed that the protein-protein
254 interaction is mediated by residues 733-793: no significant interaction could be seen between T25-RhlB
255 and T18-RNase E^{1-733}, although T25-RhlB could interact with T18-RNase E^{1-793} (and every longer CTD
256 truncation) or with T18-RNase $E^{733-793}$ about as strongly as with T18-RNase E^{1-1057} (Fig. 3E, Fig. S6C).
257 Of note, neither T18-RNase $E^{733-761}$ nor T18-RNase $E^{762-793}$ were able to restore β-galactosidase activity
258 above negative control levels when co-expressed with T25-RhlB (Fig. 3E), suggesting that the entire
259 AR1 SLiM, as defined in Fig. 1B, is necessary for interaction with RhlB.
260 Surprisingly, all T18-RNase E CTD truncations, except T18-RNase E^{1-529}, significantly interact with
261 T25-ArcB, suggesting a complex binding that is dependent on residues 529-588 (Fig. 3F, Fig. S6D). Of
262 note, these residues only contain the MTS SLiM, which is presumably involved in membrane binding.
263 Building on the bacterial two-hybrid assays results, we successively employed affinity chromatography
264 with purified proteins to investigate direct binding, minimizing the influence of other protein partners
265 or RNA. Fusion proteins containing a C-terminal 3xFlag tagged RNase E^{1-529}, RNase $E^{572-1057}$ (CTD

266 with no MTS) were purified and immobilized on anti-Flag magnetic beads. After extensive washing,
267 the beads were mixed with either purified PNPase or RhlB proteins, and the free or bound fractions
268 were analysed by SDS-PAGE (Fig. 4).
269 PNPase was retained on beads containing Flag-RNase $E^{572-1057}$, but not on beads alone or containing
270 Flag-RNase E^{1-529} (Fig. 4A), indicating that the RNase E CTD is sufficient for direct interaction with
271 PNPase. Point mutations within the NDPR SLiM (Flag-RNase $E^{572-1057}$_NDPRmut) abolished the
272 binding, confirming that this SLiM is sufficient for direct interaction, as suggested by the BTH assay
273 (Fig. 4A). Of note, PNPase is not retained on beads containing Flag-RNase E^{1-588}, which suggests that
274 residues 529-588 are not sufficient to mediate a direct protein-protein interaction, with the NDPR SLiM
275 being the major binding site (Fig. S5B). Similarly, RhlB was retained on Flag-RNase $E^{572-1057}$ but not
276 on Flag-RNase E^{1-529} and point mutations in the AR1 SLiM (Flag-RNase $E^{572-1057}$–AR1mut) showed that
277 this region is crucial for RhlB binding (Fig. 4B).
278 Contrastingly, ArcB was not retained on beads containing either Flag-RNase E^{1-1057} or Flag-RNase E^{1-}
279 ^{588} under the tested conditions, suggesting an indirect type of interaction (Fig. S5C).
280 To summarize, these experiments clearly establish PNPase and RhlB as core components of *P.*
281 *aeruginosa* RNA degradosome and demonstrate that the NDPR and AR1 SLiMs are essential for their
282 direct interactions with RNase E.
283
284 **PNPase and RhlB are dependent on their physical interaction with RNase E for colocalising in**
285 **RNA degradosome foci.**
286 Given the foci localization of RNase E, we assessed PNPase and RhlB colocalization with RNase E by
287 using *P. aeruginosa* strains carrying *rne::mCherry* and either *pnp::msfGFP* or *rhl::msfGFP*
288 chromosomal fusions. As expected, both PNPase-msfGFP and RhlB-msfGFP formed foci near the
289 membrane and co-localized with RNase E-mCherry in live cells (Fig. 5A). Overlap coefficients between
290 the two fluorescence channels were consistently over 0.9, while Pearson's coefficients were slightly
291 lower (0.880 for PNPase and 0.773 for RhlB), likely due to differences in signal intensity. Of note,
292 strains expressing any of these chromosomal fusion proteins grow identically to the WT strain at 37°C,
293 suggesting that all the fusion proteins are functional (Figure S7A). We also assessed the subcellular

294 localisation of ArcB-msfGFP and observed a smooth distribution rather than foci, which suggests that
295 the interaction between RNase E and ArcB is likely transient, with ArcB not being a core component of
296 the complex (Fig. S7C).
297 To further corroborate the need for specific RNase E domains in these interactions, we examined the
298 localization of PNPase-msfGFP and RhlB-msfGFP in strains expressing RNase E^{1-1057} (WT), RNase E^{1-}
299 ^{529} (*rne529*), RNase E^{AR1mut} (*rne*$AR1^{mut}$), or RNase $E^{NDPRmut}$ (*rne*$NDPR^{mut}$). Both PNPase-msfGFP and
300 RhlB-msfGFP displayed diffuse cytosolic localization in the *rne529* strain compared to the WT strain
301 (Fig. 5B). In the *rne*$NDPR^{mut}$ strain, PNPase-msfGFP showed a diffuse cytosolic distribution, while
302 RhlB-msfGFP was diffuse in the *rne*$AR1^{mut}$ strain, highlighting an impaired recruitment into the RNase
303 E foci. However, the NDPR or AR1 mutations did not prevent the other protein partner from being
304 recruited into the foci, indicating that both proteins can be independently recruited into RNase E-driven
305 foci (Fig. 5B). We also confirmed that RNase E NDPRmut-msfGFP forms foci, ruling out the possibility
306 that the loss of PNPase foci in the *rne*$NDPR^{mut}$ strain is due to impairment of RNase E-driven foci
307 formation (Figure S7B). These findings confirm the *in vivo* interaction of Pa PNPase and Pa RhlB with
308 the NDPR and AR1 SLiMs, respectively, and demonstrate that these interactions are crucial for their
309 near-membrane foci localization.
310

311 **Phenotypic changes associated with partial or complete deletion of RNase E CTD**

312 To investigate the biological importance of RNase E CTD-mediated complex scaffolding in *P.*
313 *aeruginosa*, we performed some phenotypic assays using the *rne529* and *rne588* strains, as well as
314 strains bearing the AR1 mutation (*rne*$AR1^{mut}$), NDPR mutation (*rne*$NDPR^{mut}$), or AR1+AR4+REER
315 mutation (*rne*AR1+AR4+$REER^{mut}$), abolishing RhlB binding, PNPase binding, or CTD-mediated RNA
316 binding plus RhlB binding, respectively.
317 On solid media at 37°C, the *rne529*, *rne588* and *rne*AR1+AR4+$REER^{mut}$ strains displayed no severe
318 growth defect but a significantly reduced colony size, suggesting a growth delay (Fig. 6A top panel,
319 Fig. 6B). Indeed, the *rne529, rne588* and *rne*AR1+AR4+$REER^{mut}$ strains exhibited a slight but
320 consistent growth delay at 37°C in liquid culture (Fig. 6C). To verify that the growth delay was caused
321 by truncations/mutations introduced in the *rne* gene, we electroporated the WT or the two most impaired

322 mutant strains with an inducible vector allowing in-trans expression of RNase E, RNase E-msfGFP, or
323 RNase E-mCherry. Cultivation of the strains at 37°C in liquid culture revealed that expression of either
324 native or fluorescently-tagged RNase E could restore identical growth levels compared to the
325 electroporated WT strain, additionally confirming that the fluorescently-tagged RNase E protein is fully
326 functional (Fig S8).
327 Interestingly, when cultured on solid media at 16°C, the *rne588* strain showed impaired growth, while
328 the growth defects of the *rne529* and *rne*AR1+AR4+REER^{mut} strains became more pronounced, with
329 *rne529* barely growing (Fig. 6A, upper middle panel). Since the *rne*AR1^{mut} and the *rne*NDPR^{mut} strains
330 exhibited no significant differences compared to the WT, these results indicate that the cold sensitivity
331 of the *rne588* strain can be attributed to the loss of RNase E CTD RNA binding. Moreover, the severe
332 growth defect observed in the *rne529* mutant indicates that additional delocalisation of RNase E from
333 the membrane exacerbates the cold sensitivity caused by deletion of RNase E RNA-binding SLiMs.
334 Besides low temperature, we also tested sensitivity to low or high pH (Fig. 6A, lower panels): while
335 growth at pH≃9.5 is rather similar between the different strains, deletion of the CTD (*rne529* and
336 *rne588*) impairs growth at pH≃5.5, although the three CTD point mutant strains are mostly unaffected.
337 This suggests that, although loss of interaction with PNPase or RhlB separately does not seem to impair
338 growth, the combined loss of RNase E protein-protein and protein-RNA interactions results in a growth
339 defect under low pH conditions. Finally, we assessed whether the RNase E CTD mutants might be
340 impaired in virulence using *Galleria mellonella* larvae, a highly predictive infection model for studying
341 mammalian infection processes [66]. Infection with PAO1 WT, *rne*AR1^{mut} and *rne*NDPR^{mut} strains
342 resulted in nearly 100% larval mortality within 20 hours post-injection (Fig 6D). In contrast, the larvae
343 infected with the *rne588* mutant exhibited 50% survival at this time point, while those infected with
344 *rne*AR1+AR4+REER^{mut} or *rne529* mutants showed 100% survival, with larval death occurring only
345 after 21 hours post-injection (Fig 6D). These results strongly indicate that the ability of *P. aeruginosa*
346 to infect a host is compromised when RNase E CTD-mediated RNA binding is disrupted. This
347 impairment is likely attributable to several contributing elements: reduced bacterial growth within the
348 host, deficiencies in virulence factor production, and a decreased ability to endure host immune
349 responses and host-related stresses.

350

351 **Effect of RNase E CTD on *P. aeruginosa* transcripts steady-state levels**

352 To better understand the phenotypes observed and evaluate the impact of RNase E CTD loss on *P.*
353 *aeruginosa* transcriptome, we conducted RNA-sequencing analysis on *P. aeruginosa* WT, *rne529,* and
354 *rne588* mutant strains grown at 37°C until the late-exponential growth phase (OD_{600nm} of 1-1.2).
355 Biological triplicates were analysed and show a high degree of relatedness within each strain (Fig. S9A-
356 B). Under these conditions, the loss of the entire RNase E CTD in the *rne529* strain affected the steady-
357 state levels of 450 transcripts, with 183 downregulated and 267 upregulated (adjusted p-value < 0.05,
358 fold change $|FC| \geq 2$) (Fig. 7A). In the *rne588* mutant, 417 transcripts were differentially expressed,
359 with 194 downregulated and 223 upregulated (adjusted p-value < 0.05, fold change $|FC| \geq 2$) (Fig. 7B).
360 Differential expression analysis on reads mapping to predicted small RNA genes (sRNAs) identified 14
361 predicted sRNA genes with significantly enriched reads in the *rne529* mutant and 5 in the *rne588* strain
362 (Table S5).

363 A comparison of the *rne529* and *rne588* strains revealed that 164 mRNAs were consistently regulated
364 in both mutants (97 upregulated and 67 downregulated, see Figure 7C). Among the strongest commonly
365 downregulated genes were: (i) the *pqsABCD*, *pqsE*, and *pqsH* genes, involved in the synthesis of
366 quorum-sensing signal molecules alkylquinolones PQS (2-heptyl-3-hydroxy-4(1H)-quinolone) and
367 HHQ (2-heptyl-4(1H)-quinolone), which play roles in virulence [67], (ii) the *phzA1B1* and *phzA2B2*
368 phenazine biosynthesis genes, which are important for synthesis of the toxic secondary metabolites
369 phenazine and pyocyanin [68], and (iii) the *agtABCD* gene cluster for 4-aminobutyrate (GABA) and 5-
370 aminovalerate (AMV) uptake [69]. Surprisingly, the two strains exhibited more differences in mRNA
371 levels than shared changes. In the *rne588* strain, the mRNA levels corresponding to type 3 secretion
372 system genes, which deliver toxins to host cells [70], were consistently upregulated, while they did not
373 vary significantly in the *rne529* strain as compared to the WT (Fig 7D). On the other hand, ribosomal
374 and many amino acid metabolism genes (tryptophan, arginine, alanine, aspartate and glutamate) were
375 downregulated only in the *rne529* strain, which could correlate with the general growth defect observed
376 (Fig. 7E and Table S5).

377 Considering the autoregulation of RNase E reported in *E. coli* and *C. crescentus* [63, 71], we quantified
378 reads mapping to the 5' untranslated region (UTR) of the *rne* gene (transcription start site determined
379 in [72]) and observed increases of 2 and 0.96 $\log_2$ folds in the *rne529* and *rne588* mutants, respectively,
380 compared to the WT (Fig. 7F). Similarly, we observed a 1.43 and 0.88 $\log_2$ fold increase in the transcript
381 corresponding to the NTD of RNase E in the *rne529* and *rne588* mutants, respectively (Fig. 7F), in
382 agreement with the observed increase in protein levels (Fig. S4C-D).
383 Finally, to assess RNA degradation efficiency in our strains, we analysed the 5' reads ends of sequenced
384 RNA fragments. As previously performed in other studies [56, 73], we calculated the ratio between the
385 number of loci with 5' ends present only in a mutant and not in the WT, over the sum of loci with 5'
386 read ends seen in both mutant and WT. We performed the analysis in the three genetic backgrounds
387 (WT, *rne529*, *rne588*) and for each replica independently to ensure consistency (see methods and Fig
388 S10). Despite the background of random fragmentation intrinsic to the sequencing protocol, a consistent
389 increase on the number of 5' ends in the *rne529* and *rne588* strains was observed as compared to the
390 WT (Fig. 7G), suggesting an accumulation of RNA degradation intermediates and an altered RNA
391 degradation in the RNase E truncated mutants.
392
393 **Discussion**
394 The composition and the functions of the RNA degradosome vary among bacterial species, likely
395 reflecting diverse lifestyles and niche adaptations [30]. Studying the RNA degradosome in various
396 bacterial species is therefore crucial for elucidating how bacteria respond and adapt to different
397 environmental conditions and sustain various types of stress. In this study, we characterized the RNA
398 degradosome of *P. aeruginosa*, a versatile opportunistic pathogen and widely used model organism for
399 bacterial pathogenesis and environmental adaptation.
400 In the first part of our study, we focused on the putative SLiMs within the CTD of *P. aeruginosa* RNase
401 E and assessed their contribution to RNA binding and foci assembly. We successively identified RhlB
402 and PNPase as core RNA degradosome components, as well as the SLiMs mediating these interactions
403 (Fig. 8). A notable feature of SLiMs is their poor sequence conservation, even when they mediate

404 interactions with the same protein partner. Our findings confirm this variability for both PNPase and
405 RhlB interactions.
406 PNPase, a known partner of RNase E in several species, binds through SLiMs with significantly
407 different sequences across organisms. For instance, in *Anabaena* PCC7120, the interaction occurs via a
408 cyanobacterial SLiM having the conserved residues RRRRRRSSA [37], while in *E. coli* or *C.*
409 *crescentus*, the sequences are WQRPTFAFEGKGAAGGHTATHHASA [30] and
410 APPEKPRRGWWRR [43], respectively. Our pull-down assays and *in vitro* binding assays showed that
411 PNPase interacts with RNase E in *P. aeruginosa* via the NDPR SLiM, which has yet another distinct
412 sequence (TGRALNDPREKRRLQREAERLAREAAAAA). These sequence variations may reflect
413 species-specific interactions, as suggested by experimental work showing lack of heterologous
414 interactions between RNase E and PNPase of *E. coli* and *Pseudoalteromonas haloplanktis* [42]. Despite
415 sequence variability, the PNPase interacting SLiM is consistently located towards the end of the RNase
416 E CTD [30, 37, 43], suggesting convergent evolution in the positioning of the PNPase relative to other
417 RNA degradosome components and to RNase E catalytic domain.
418 Of note, a recent study on a *P. aeruginosa* mutant with a 50 bp deletion in the 3' end of the *rne* gene
419 revealed a hypervirulence phenotype, characterized by enhanced cytotoxicity and siderophore
420 production [74]. Based on *E. coli* RNA degradosome model, this phenotype was associated with a
421 possible impairment of PNPase binding to Pa RNase E or a different RNA degradosome activity [74].
422 Our data reveal that PNPase can interact with the RNase E^{1-1025} truncation (BTH assay), ruling out the
423 former hypothesis. However, we cannot exclude the possibility that this region might be involved in
424 interaction with a yet unknown partner.
425 Regarding RhlB, we show that in *P. aeruginosa*, this RNA helicase directly interacts with RNase E via
426 the AR1 SLiM (RPRRRSRGQRRRSNRRERQR). Mutation of AR1 disrupts not only the RhlB-RNase
427 E binding *in vitro*, but also RhlB subcellular localisation near the membrane and co-localization with
428 RNase E *in vivo*. Interestingly, in *E. coli* and other species the AR1 SLiM mediates RNA interaction
429 [30, 42]. In *P. aeruginosa*, AR1 also contributes to RNA-binding in addition to RhlB binding. Given
430 that in *E. coli,* a single arginine mutation within the HBS SLiM (R730A) is sufficient to disrupt RhlB
431 binding [75], it is possible that only one or a few arginine residues of the AR1 SLiM are involved in

interaction with RhlB, while the others mediate RNA binding. Further experiments are needed to address this hypothesis and to understand the dynamics of the RhlB-RNA-RNase E complex in *P. aeruginosa*. Moreover, it has been shown that the RNA-dependent ATPase and unwinding activity of RhlB are stimulated by binding to RNase E [76]. Future studies will investigate whether it is also the case in *P. aeruginosa*.

In contrast with the *E. coli* RNA degradosome, we did not find any evidence of an interaction between RNase E and enolase in *P. aeruginosa* when the bacteria grow in rich medium and standard laboratory conditions. Although our pull-down and bacterial-two hybrid data indicate a probable interaction between RNase E and ArcB, a catabolic ornithine carbamoyltransferase from the arginine deaminase pathway [77], no direct protein-protein binding could be observed *in vitro,* nor were the two proteins colocalising in vivo. We propose that RNase E indirectly interacts with ArcB, probably in a RNA-dependent manner. Indeed, the *P. aeruginosa arcDABC* polycistronic transcript undergoes endonucleolytic cleavage at multiple sites for its processing [78], suggesting that an regulatory interaction between RNase E and ArcB polypeptide could occur during co-translational RNA cleavage [18].

Additionally, the RNase E-based RNA degradosome of *P. haloplanktis, P. syringae*, and *R. capsulatus* do not seem to contain either a metabolic enzyme upon standard growing conditions [40-42]. This lack of RNase E interaction with metabolic enzymes may reflect distinct physiological roles of the RNA degradosome in different bacterial species, potentially linked to specific metabolic adaptations or regulatory mechanisms that modulate RNA stability and processing depending on nutrient availability. However, we cannot exclude that some protein partners were missed as we chose a stringent threshold for analysis of the pull-down results. Transient or condition-specific accessory protein partners remain to be identified, and compositional biases such as the conserved AEPV-rich part of the RNase E CTD are not yet understood, as no ligand or biological function has been assigned to this region even in well-studied RNase E orthologs.

It is also important to mention that throughout this study, we chose to focus on core RNA degradosome components that are identified based on their binding to RNase E CTD, but we cannot exclude that some functional interactions occur with the NTD. For example, RhlB was found to interact with RNase

460 E NTD in *C. crescentus* [36], while in *Anabaena* the RNA helicase CrhB, RNase II and enolase were
461 shown to associate with RNase E via its NTD [38, 39]. Similarly, we found that the *P. aeruginosa*
462 RhlE2 RNA helicase, previously shown to associate with RNase E in an RNA-dependent manner [55],
463 interacts with the N-terminal domain of Pa RNase E. Although RhlE2 is not considered a core RNA
464 degradosome component based on our assumption of CTD-mediated interactions, this association
465 remains functionally significant [55, 56].
466 In the second part of our study, we evaluated the importance of RNA degradosome assembly at both
467 transcriptomic and phenotypic levels through an analysis of *P. aeruginosa* strains carrying RNase E
468 CTD truncations and mutations. Comparing the *rne588* and *rne529* strains allows us to discuss the
469 importance of RNA degradosome assembly and membrane attachment in *P. aeruginosa*. The two
470 mutants exhibited varying degrees of sensitivity to cold growth, with *rne529* being the most affected,
471 indicating that cold growth requires both RNase E membrane attachment and RNA degradosome
472 assembly. Loss of the CTD without delocalisation from the membrane (*rne588*) does not affect growth
473 in *P. aeruginosa* under standard laboratory condition (i.e., 37°C and rich medium), but impacts its
474 capacity to sustain growth in the cold. Transcripts levels were also generally affected in the mutants, as
475 well as global RNA degradation, as shown in the 5' read ends analysis. Decreased degradation of
476 cleaved transcripts could lead to an upregulation of their levels. Therefore, direct and indirect effects
477 remain to be distinguished and those changes remain to be correlated with proteins levels.
478 Surprisingly, we did not find any phenotypic changes associated to the loss of RhlB or PNPase binding,
479 questioning the importance of the RNA degradosome protein association for the complex functionality.
480 Competition assays could be useful in identifying any fitness defects in our mutants, as done in *E. coli*
481 for RNase E CTD truncations [19, 62], or different phenotypes or stresses could be tested.
482 On the other hand, our phenotypic analysis highlights the crucial role of CTD RNA binding for the
483 functionality of the RNA degradosome complex. Mutations in the SLiMs responsible for RNA binding
484 (AR1, AR4, and the REER-repeats) not only impair *in vivo* RNA degradosome foci assembly and/or
485 stability but also lead to decreased *P. aeruginosa* virulence and reduced growth at both 37°C and cold
486 temperatures. The effect of these mutations on foci formation mirrors the effect observed upon cell
487 exposure to rifampicin, which decreases RNA levels in the cell, and aligns with previous studies

488 showing that Ec and Cc RNase E orthologs also assemble foci in a CTD-dependent and RNA-dependent
489 manner [60-62]. Our data thus suggest that impairing foci formation has a major effect on the activity
490 of the RNA degradosome in *P. aeruginosa*.
491 Overall, our study identified core RNA degradosome components in *P. aeruginosa* and underscores the
492 role of this complex in bacterial adaptation to environmental changes and pathogenesis. By revealing
493 *P. aeruginosa*-specific interactions and their functional significance, our findings provide valuable
494 insights into the molecular mechanisms of adaptation in this pathogen and highlight the potential of the
495 RNA degradosome as a drug target.
496

497 **Methods**

498 **Bacterial strains and growing conditions**

499 A list of bacterial strains used can be found in Table S1. Unless otherwise specified, *P. aeruginosa* PAO1
500 was grown at 37°C in NYB (25 g of Difco nutrient broth, 5g of Difco yeast agar per liter) with shaking
501 at 180 rpm or on Nutrient Agar (NA) (40 g Oxoid blood agar base, 5 g Difco yeast agar per liter). When
502 required, antibiotics were added to these media at the following concentrations: 100 µg/ml ampicillin,
503 50 µg/mL kanamycin, 20 µg/mL tetracycline and 10 µg/ml gentamicin for *E. coli*; and 50 µg/mL or 100
504 µg/mL tetracycline and 50 µg/ml gentamicin for *P. aeruginosa*.
505

506 **Construction of plasmids used in this study**

507 Information about plasmid construction and primers used in this study can be found in supplementary
508 tables S2 and S3, respectively. Plasmids pUT18C and pKT25 were generally cloned by restriction
509 enzyme digestion using EcoRI-HF and BamHI-HF (NEB). When a gene to be inserted could be
510 internally cleaved by EcoRI and/or BamHI, the enzymes MfeI and/or BglII, respectively, were chosen
511 instead during primer design to allow ligation of the insert to the vector digested with EcoRI/BamHI
512 thanks to compatible cohesive ends. For cloning of *gdhB* into pKT25, NEB assembly® was used instead,
513 due to the presence of many restriction enzymes internal cleavage sites. Ligation reactions were carried
514 our using T4 DNA ligase (Roche or NEB) at 16°C overnight, or at room temperature for 2-3 hours,
515 following standard protocols. When cloning inserts into the suicide vectors pME3087 or pEXG2, the

516 NEBuilder HiFi DNA assembly Master Mix (NEB) was used according to the manufacturer's
517 recommendations. To constructs RNase E CTD mutants, the DNA was synthesized by GeneArt
518 (ThermoFisher Scientific) and cloned into appropriate vectors for protein purification or strain
519 construction. A description of the introduced mutations can be found in Table S4. To construct
520 pME6032-based expression vectors, restriction enzyme digestion was carried out using EcoRI and KpnI
521 for both vector and inserts.
522 Ligation mixtures or the assembly reactions were transformed into chemically competent *E. coli* DH5α
523 cells by heat-shock, plating on appropriate selective LB agar medium. The resulting colonies were
524 screened by PCR for the presence of the insert in the plasmid of interest. After plasmid extraction
525 (Miniprep kit, Sigma-Aldrich/Merck), plasmids were verified by Sanger sequencing at Microsynth.
526
527 **Construction of *P. aeruginosa* mutant strains**
528 To construct chromosomal gene truncations or insert a Strep-tag or fluorescent protein into the
529 chromosome, in frame with a gene of interest, the suicide vectors pEXG2 [79] or pME3087 [80] were
530 used. Briefly, approximately 500 bp regions located immediately upstream or downstream of the region
531 to be edited, and, when applicable, the tag or fluorescent protein of interest, were amplified by PCR and
532 inserted together into the vector backbone using NEB assembly®. After sequencing verification of the
533 constructed plasmid quality, the plasmids were introduced into *P. aeruginosa* PAO1 strain by triparental
534 mating using the *E. coli* strain HB101 (pRK2013). After selection with the appropriate antibiotic
535 (tetracycline for pME3087 or gentamicin for pEXG2), merodiploids were resolved as described in [81]
536 for pME3087 or [79] for pEXG2, and strains with the desired insertion/deletion were identified by
537 colony PCR.
538
539 **RNase E sequence analysis**
540 Group-specific homologs of RNase E in *P. aeruginosa*, *P. fluorescens*, *P. protegens*, *P. putida* and *P.*
541 *stutzeri* were retrieved from NCBI databases using blastp [82] with *P. aeruginosa* PAO1 RNase E as a
542 query; only sequences with query coverage > 0.5 were conserved (total of 5000 proteins). The number
543 of RE[E/D]R motifs in each protein sequence was determined using the vcountPattern function from

544 the “biostrings” R package [83]. The similarity of the protein sequences within a taxonomic group was
545 determined using the conserv function (method=“similarity”) from the bio3D R package on a muscle
546 alignment of the protein sequences[84, 85].
547
548 **Electrophoretic motility shift assay**
549 The *malEF* transcript was synthesized with a T7 transcription kit (Invitrogen) on linear DNA template
550 (172 bp) obtained by PCR with primers p253-p254 (see Table S3). The electrophoretic mobility shift
551 assay (EMSA) was performed following the protocol of [86]. Briefly, the reaction mixtures (15 µl)
552 contained 35 nM of RNA, 50mM Tris-HCl, 100mM NaCl, 5mM DTT, 1.0 units/µl RNasin (Promega),
553 and His10Smt3-RNase E proteins as specified, with protein concentration expressed as a molar ratio of
554 relative to RNA concentration (see Fig. 2A and S4A-B).
555 The reactions were incubated at 4 °C for 30 min before loading on 2% agarose gel and run at 150 V for
556 15 min. RNA bands were visualized by gel staining with SybrGold (Invitrogen).
557
558 **Epifluorescence microscopy imaging**
559 Phase contrast and fluorescence microscopy were performed on a Zeiss Axio Imager 2 equipped with
560 an objective alpha Plan-Apochromat 100x/1,46 Oil Ph3 M27 and a ZEISS Axiocam 305 mono CCD
561 camera. Bacteria were grown until OD_{600nm}= 0.2-0.6 (approx. 2.5 hours) in 3 ml of NYB and were then
562 placed on an agarose pad containing 1% agarose dissolved in 0.5X PBS. Images were processed with
563 Fiji (NIH, USA) [87].
564
565 **Image analysis**
566 All image treatments and analysis were performed using Fiji (NIH, USA)[87]. Representative images
567 shown had contrast adjusted for display by opening the images in Fiji and using the Reset function in
568 the Adjust Brightness/Contrast menu, after average background intensity subtraction using the Math ->
569 Subtract function. These average background intensity values were obtained by measuring a square area
570 devoid of any cells.

571 For quantification of signal intensity in Fiji, a line was drawn along the longitudinal axis of bacterial
572 cells and signal was measured using Plot Profile. Results of this function were saved as .csv files. For
573 each strain, at least 50 bacterial cells were measured from the raw images, using at least two different
574 images for quantification. Average background values were subsequently subtracted from each results
575 file using a .csv file containing the Plot Profile measurements of a linear area devoid of cells for each
576 image used. Boxplots of fluorescence intensity and signal variance or pooled histograms were plotted
577 using R [88]. The signal variance was obtained by calculating the variance of the $\log_2$ fold-change
578 between each measured value and the average of all values for a given measured cell. This was done to
579 normalize the data and obtain comparable variances without introducing a bias due to differences in
580 overall signal intensity.
581
582 **Pull-down identification of RNase E partners**
583 Fresh cultures of PAO1 WT, PAO1 RNase E_{1-529}-Strep, or PAO1 RNase E_{1-1057}-Strep were inoculated to
584 OD=0.05 from overnight cultures in 500 mL Erlenmeyer flasks. Cultures were grown until approx.
585 OD_{600nm}=0.8-0.9. 50 mL of each culture was harvested by centrifugation at 4500 *x g* for 10 minutes.
586 Pellets were stored at -80°C until needed.
587 Each thawed pellet was then resuspended in 3,25 mL of lysis buffer (for 10 mL of buffer, prepared just
588 before use: 20 mM Tris (pH 10), 250 mM NaCl, 10% v/v glycerol, 1 EDTA-free protease inhibitor
589 tablet, 50 µg/mL lysozyme). Samples were incubated the samples on ice for about 30 minutes,
590 transferred into 15-mL Falcon tubes and sonicated using a thin probe for 6x30s, with 15 seconds break
591 in between. A pulse of 70% and a power output of 50% were used. After sonication, 32.5 µL of Triton
592 X100 10% were added to each sample (~0.1% final) before incubation on a rotary wheel at 4°C for 8
593 minutes. The samples were transferred into 2 mL Eppendorf tubes and centrifuged for 1 hour at 10500
594 *x g* at 4°C. MagStrep® Strep-Tactin®XT beads (IBA, cat# 2-5090) were washed in wash buffer (20 mM
595 Tris (pH 10), 250 mM NaCl, 10% v/v glycerol) according to the manufacturer's instructions. One mix
596 of beads was prepared for all the samples with a volume of beads suspension of 45 µL per sample. Final
597 resuspension was done in 200 µL wash buffer per sample, plus an additional 10 µL. After centrifugation
598 of the samples, the supernatant of each sample was regrouped into a 5 mL Eppendorf tube, and 200 µL

599 of washed beads suspension were added per sample. Incubation on a rotary wheel was done for 2h15 at
600 4°C. The 5 mL tubes were then placed against a magnetic rack and all the supernatant was carefully
601 removed. A first wash volume of 500 µL was added gently and agitated by horizontal rotations of the
602 tubes. Tubes were placed back against the magnetic rack and the wash volume was removed. A second
603 wash step was performed identically with a volume of 225 µL instead of 500 µL. A third wash step of
604 225 µL was also performed, and the resuspended beads were transferred into a clean 1.5 mL Eppendorf
605 tube by gentle pipetting with a 1000 µL tip, before removing the wash volume. The beads were covered
606 with 10 µL of sterile PBS and stored at 4°C before LC-MS/MS analysis at the Proteomics Core Facility
607 (University of Geneva). For plots in Fig. 3A-B, the log2 fold-change (log2FC) was calculated using the
608 following formula: log2(average peptide count of protein *x* identified in the RNase $E^{1\text{-}xxx}$-Strep / average
609 peptide count of protein *x* identified in the untagged sample).When an average count of 0 peptide was
610 identified in the untagged sample, the log2FC value was instead calculated using the following formula:
611 log2FC(average peptide count of protein *x* identified in the RNase $E^{1\text{-}xxx}$-Strep/1).
612
613 **Bacterial adenylate cyclase two-hybrid assay**
614 Cloned plasmids were introduced into chemically competent BTH101 cells by heat shock, and the cells
615 were plated in LB agar supplemented with ampicillin and kanamycin. Isolated colonies were then
616 streaked as a line of about 1-2 cm on freshly prepared Mac Conkey agar medium supplemented with
617 ampicillin, kanamycin, 0.5 mM isopropyl β-d-thiogalactoside (IPTG), and maltose 1%. The
618 MacConkey Petri dishes were then incubated at 30°C for 24h followed by an incubation at room
619 temperature (~23°C) for 24h. The bacteria were imaged by scanning the plates, after which
620 quantification of β-galactosidase activity was done using ONPG as described in [89].
621
622 **Protein purification**
623 His_{10}Smt3-tagged PNPase, His_{10}Smt3-tagged RhlB, and His_{10}Smt3-tagged ArcB proteins were purified
624 from soluble bacterial lysates by nickel-agarose affinity chromatography as described previously in the
625 supplementary information of Hausmann *et al.* 2021 [55]. The imidazole elution profiles were
626 monitored by SDS-PAGE. The recombinant His_{10}Smt3-tagged proteins were recovered predominantly

627 in the 250 mM imidazole fraction. Protein concentration was determined using the Bio-Rad dye reagent,
628 with BSA as the standard, and calculated by interpolation against the BSA standard curve. The His_{10}-
629 Smt3 tag remained uncleaved in the protein-protein interaction assays.
630 RNase E^{1-1057}, RNase E^{1-588}, RNase E^{1-529}, RNase $E^{572-1057}$, RNase $E^{572-1057_NDPRmut}$, and RNase E^{572-}
631 ^{1057_AR1mut} proteins, each carrying a His_{10}Smt3 tag at the N-terminus and a Twin-Strep-tag®-Flag at the
632 C-terminus, were purified as described above. The 250 mM imidazole elution fractions were used
633 directly in the Protein-Protein interaction assays. For the EMSA experiment, the RNase E proteins were
634 further purified as follows: the 250 mM imidazole fraction were applied to a 1 ml of Strep-Tactin
635 Sepharose (Iba) column that had been equilibrated with buffer C (50 mM Tris pH8, 200 mM NaCl, 10
636 % glycerol). The column was washed with 5 ml of buffer C and then eluted stepwise with 1 ml aliquots
637 of buffer C containing, 2.5 mM D-Desthiobiotin respectively. The elution profiles were monitored by
638 SDS-PAGE.
639
640 **Protein-protein interaction assays**
641 Anti-Flag M2 magnetic beads (Sigma M8823) were used for the binding assay. Unless otherwise
642 specified, a volume of 25 µL of beads suspension was used per reaction sample. The beads were washed
643 once with 1 mL of buffer H (50 mM Tris-HCl, pH 8.0, 150 mM NaCl, 0.01% Triton X-100), before
644 being resuspended in fresh buffer H and aliquoted into one Eppendorf tube per sample. Purified RNase
645 E^{1-529}-Flag, RNase E^{1-588}-Flag RNase $E^{572-1057}$-Flag, RNase $E^{572-1057_NDPRmut}$- Flag, or RNase E^{572-}
646 ^{1057_AR1mut}- Flag fusion proteins (20-25 µg each) were diluted in buffer H to a final volume of 100 µL
647 and incubated with the magnetic beads for 1 hour at 4 °C on a rotating device. When using purified
648 RNase E^{1-1057}-Flag fusion protein instead, a volume of 450 µL of purified protein (in a buffer with 50
649 mM Tris pH=8, 500 mM NaCl, 10% glycerol and 250 mM imidazole) was incubated with 50 µl of Anti-
650 Flag M2 magnetic beads (Sigma M8823). After the incubation, the beads were collected using a
651 magnetic separator and washed three times with 0.25 ml of binding buffer H to remove any unbound
652 protein.
653 For affinity chromatography, the anti-Flag magnetic beads (Sigma-Aldrich) with bound RNase E-Flag
654 fusion proteins, or unbound beads, were incubated with either 5 µg of PNPase (Figure 4A), 5 µg of

655 RhlB (Figure 4B), or 5 µg of ArcB diluted in buffer H (final volume 100 µL, 50 µl of beads suspension
656 used for probing ArcB binding) for 1 hour at 4 °C on a rotating device. After incubation, the beads were
657 collected using the magnet, and the supernatant (free fraction F) was withdrawn. The anti-Flag beads
658 were then resuspended in 100 µl of binding buffer H and subjected to three rounds of washing of 100
659 µl each. Following the final wash, the proteins bound to the beads were eluted with 100 µl of 2X LDS
660 sample buffer (Invitrogen) supplemented with 167 mM DTT. Aliquots (15 µl) of the input protein
661 sample (PNPase or RhlB), the first supernatant fraction (free fraction F), and the bead-bound fraction
662 were mixed with 5 µl of 4X LDS sample buffer (Invitrogen), heated at 80 °C for 5 minutes, and analysed
663 by SDS-PAGE. Polypeptides were visualized using Coomassie Blue staining.
664
665 **Growth assays on solid or liquid media**
666 To assess the growth of the mutant strains in liquid medium, 200 µL of NYB broth was inoculated to
667 OD_{600nm}=0.05 in a 96-well plate, using an overnight culture washed twice with fresh medium. The wells
668 on the edge of the plate were not used. The plate was incubated at 37°C using a Biotek Synergy H1
669 Hybrid Plate reader. OD_{600nm} values were measured every 30 minutes. Before each OD_{600nm}
670 measurement, orbital shaking with 282 cpm (3 mm) was performed for 1 minute. Data was retrieved
671 the following day and plotted after substraction of blank OD_{600nm} values using GraphPad Prism.
672 When growing strains carrying the pME6032 vector for complementation assays, NYB medium was
673 supplemented with 50 µg/mL of Tetracycline and 70 µM of IPTG for induction. Cells were resuspended
674 in supplemented NYB after washing and before inoculating the 96-well plate.
675 To assess the growth of the mutant strains on solid medium, square Petri dishes (12x12cm) were filled
676 with 50 mL of warm NA. When testing growth at low vs high pH, either 75 µL of 37% fuming HCl or
677 400 µL of 5N NaOH was added per 50 mL of NA agar to achieve the desired conditions. A fresh culture
678 (OD_{600nm}= 0.4-0.8) of each strain was adjusted to OD_{600nm}=1 by centrifugation and serially diluted in a
679 96-well plate using a multipipette. 5 µL of each dilution series was then spotted using a multipipette
680 onto pre-dried NA plates (1 hour under a sterile flowhood). After the spots had dried, plates were
681 incubated upside down at 37°C or 16°C.
682

683 **Galleria killing assays**

684 *Galleria mellonella* larvae were used to assess in vivo virulence and/or survival of several RNase E
685 mutant strains. Fresh cultures were adjusted to a suspension of OD_{600nm}= 1 and serially diluted to 10^{-6}
686 in Gibco Dulbecco's Phosphate Buffered Saline (dPBS) (Thermo Fisher Scientific). 10 µL of the 10^{-6}
687 dilution were spotted onto NYB agar to verify that the dilutions were similar for the different strains.
688 10 µL spots were then put onto a clean parafilm and injected using Omnican 50 sterile insulin syringe
689 (Braun) into the second to last leg of the larvae, facing towards the head. As a control, sterile dPBS was
690 injected similarly into larvae to assess background levels of death. For every 10 larvae injected, the time
691 of injection was recorded, and they were placed inside a dark incubator at 37°C. The next day, deaths
692 were recorded every hour. A larva was considered dead when it completely stopped responding to
693 stimuli (touched on the legs or the head with a pipette tip). Time of death was calculated as the interval
694 of time between recorded time of injection and death occurence. Survival curves were plotted and
695 analysed with GraphPad Prism (GraphPad Software, Prism10.2).

696

697 **RNA-seq sample collection**

698 Independent triplicates cultures of PAO1 WT, PAO1 RNase E_{1-588}, (*rne588*) and PAO1 RNase E_{1-529}
699 (*rne529*) strains were grown in 50 mL Erlenmeyer flasks (10 mL NYB broth) until OD_{600nm}= 1.0-1.2.
700 500 µL of each culture were immediately added into four separate 1.5 mL tubes, each containing 1 mL
701 of RNAlater (Sigma-Aldrich, cat). After harvesting of all three strains, the tubes were centrifuged for
702 30 minutes at 9600 x *g*. Supernatant was discarded and pellets were stored at -80°C until RNA
703 extraction. The RNA extraction was performed using two tubes of pellets for each strain and replicate,
704 with the Monarch Total RNA Miniprep kit. For lysis of the bacterial cells, the two pellets were
705 resuspended in 250 µL of 1X Tris-EDTA (TE) buffer supplemented with 1 mg/mL of lysozyme and
706 regrouped into one tube for each strain, incubated for 5 minutes at RT, and RNA was subsequently
707 extracted following the manufacturer's instructions. After RNA purification, an additional DNA
708 removal treatment was done using TURBO DNase (Thermo Fisher) according to the manufacturer's
709 instructions. RNA was purified again using the RNA purification columns (dark blue) from the Monarch
710 Total RNA Miniprep kit, and following the priming, washing and elution steps described by the

711 manufacturer. The absence of residual gDNA contamination was verified by performing a PCR for 35
712 cycles using primer pairs targeting *rpoD* [55]. Biological triplicate samples for each strain were
713 prepared. Quality check, ribosomal RNA depletion and RNA sequencing were conducted by Novogene.
714

715 **RNA sequencing analysis**

716 Reads were mapped using Bowtie2 [90] to *Pseudomonas aeruginosa* PAO1 genome assembly
717 ASM676v1 and counts were aggregated using summarize Overlaps in the package GenomicAlignments
718 [91] in R using the ASM676v1 gtf version 2.2 (NCBI accession: GCF_000006765.1). Differential
719 expression was performed using DESeq2 [92] and transcripts were considered differentially expressed
720 between two conditions if the absolute value of log2FC between conditions was greater than 1 (i.e. 2-
721 fold up or down) with a adjusted p-value less than 0.05. To find functional enrichment among
722 differentially expressed genes groups, the Kyoto Encyclopedia of Genes and Genomes (KEGG) was
723 used for gene set definitions, downloaded using the package KEGGREST [93] in R. Enrichment was
724 calculated using a hypergeometric test. All correlations presented are Pearson's product moment
725 correlation coefficient. Pairwise correlations of log2 Reads Per Kilobase per Million mapped reads
726 (RPKMs) and hierarchical unsupervised clustering analysis of fold changes relative to WT demonstrate
727 the similarity in the profile of the biological replicates for each strain. Analysis of 5' read ends per loci
728 was performed as described by de Araújo et al. [94] except that each dataset read number was down-
729 sampled to 8 million.
730

731 **Acknowledgments**

732 We thank Sylvain Guex-Crosier for his assistance with RNA extraction and Nathanaël Guggenheim for
733 protein purification and assistance with cloning experiments. We also acknowledge the Proteomics Core
734 Facility and the Bioinformatics Support Platform from the University of Geneva for assistance with the
735 realisation of LC-MS-MS and bioinformatics analyses, respectively. Work in M.V. laboratory is funded
736 by Swiss National Science Foundation (PCEFP3_203343 to M.V.) and Fondation Pierre Mercier pour
737 la Science (to M.V.). D.G. work is supported by the Swiss National Science Foundation
738 (PZ00P3_180142 to D.G., 2020–2023) and the Velux Foundation (grant 1814 to P.J. and D.G., 2023).

References

1. Hui MP, Foley PL, Belasco JG. Messenger RNA Degradation in Bacterial Cells. Annual Review of Genetics. 2014;48(1):537-59. doi: 10.1146/annurev-genet-120213-092340. PubMed PMID: 25292357.
2. Celesnik H, Deana A, Belasco JG. Initiation of RNA decay in *Escherichia coli* by 5' pyrophosphate removal. Mol Cell. 2007;27(1):79-90. doi: 10.1016/j.molcel.2007.05.038. PubMed PMID: 17612492; PubMed Central PMCID: PMCPMC2196405.
3. Deana A, Celesnik H, Belasco JG. The bacterial enzyme RppH triggers messenger RNA degradation by 5' pyrophosphate removal. Nature. 2008;451(7176):355-8. doi: 10.1038/nature06475. PubMed PMID: 18202662.
4. Luciano DJ, Vasilyev N, Richards J, Serganov A, Belasco JG. Importance of a diphosphorylated intermediate for RppH-dependent RNA degradation. RNA Biol. 2018;15(6):703-6. Epub 20180529. doi: 10.1080/15476286.2018.1460995. PubMed PMID: 29619898; PubMed Central PMCID: PMCPMC6152431.
5. Tejada-Arranz A, de Crecy-Lagard V, de Reuse H. Bacterial RNA Degradosomes: Molecular Machines under Tight Control. Trends Biochem Sci. 2020;45(1):42-57. Epub 20191101. doi: 10.1016/j.tibs.2019.10.002. PubMed PMID: 31679841; PubMed Central PMCID: PMCPMC6958999.
6. Dressaire C, Picard F, Redon E, Loubière P, Queinnec I, Girbal L, Cocaign-Bousquet M. Role of mRNA stability during bacterial adaptation. PLoS One. 2013;8(3):e59059. PubMed PMID: 23516597.
7. Broglia L, Le Rhun A, Charpentier E. Methodologies for bacterial ribonuclease characterization using RNA-seq. FEMS Microbiol Rev. 2023;47(5). PubMed PMID: 37656885.
8. Ono M, Kuwano M. A conditional lethal mutation in an *Escherichia coli* strain with a longer chemical lifetime of messenger RNA. J Mol Biol. 1979;129(3):343-57. Epub 1979/04/15. doi: 10.1016/0022-2836(79)90500-x. PubMed PMID: 110942.
9. Apirion D. Isolation, genetic mapping and some characterization of a mutation in *Escherichia coli* that affects the processing of ribonuleic acid. Genetics. 1978;90(4):659-71. PubMed PMID: 369943.
10. Jain C, Deana A, Belasco JG. Consequences of RNase E scarcity in *Escherichia coli*. Molecular Microbiology. 2002;43(4):1053-64. doi: https://doi.org/10.1046/j.1365-2958.2002.02808.x.
11. Caruthers JM, Feng Y, McKay DB, Cohen SN. Retention of core catalytic functions by a conserved minimal ribonuclease E peptide that lacks the domain required for tetramer formation. J Biol Chem. 2006;281(37):27046-51. Epub 20060719. doi: 10.1074/jbc.M602467200. PubMed PMID: 16854990.

12. Callaghan AJ, Aurikko JP, Ilag LL, Günter Grossmann J, Chandran V, Kühnel K, et al. Studies of the RNA degradosome-organizing domain of the *Escherichia coli* ribonuclease RNase E. J Mol Biol. 2004;340(5):965-79. doi: 10.1016/j.jmb.2004.05.046. PubMed PMID: 15236960.

13. Carpousis AJ, Van Houwe G, Ehretsmann C, Krisch HM. Copurification of E. coli RNAase E and PNPase: evidence for a specific association between two enzymes important in RNA processing and degradation. Cell. 1994;76(5):889-900. doi: 10.1016/0092-8674(94)90363-8. PubMed PMID: 7510217.

14. Py B, Higgins CF, Krisch HM, Carpousis AJ. A DEAD-box RNA helicase in the *Escherichia coli* RNA degradosome. Nature. 1996;381(6578):169-72. doi: 10.1038/381169a0. PubMed PMID: 8610017.

15. Chandran V, Luisi BF. Recognition of enolase in the Escherichia coli RNA degradosome. J Mol Biol. 2006;358(1):8-15. Epub 20060221. doi: 10.1016/j.jmb.2006.02.012. PubMed PMID: 16516921.

16. Worrall JAR, Górna M, Crump NT, Phillips LG, Tuck AC, Price AJ, et al. Reconstitution and Analysis of the Multienzyme Escherichia coli RNA Degradosome. Journal of Molecular Biology. 2008;382(4):870-83. doi: https://doi.org/10.1016/j.jmb.2008.07.059.

17. Bandyra KJ, Bouvier M, Carpousis AJ, Luisi BF. The social fabric of the RNA degradosome. Biochim Biophys Acta. 2013;1829(6-7):514-22. Epub 20130228. doi: 10.1016/j.bbagrm.2013.02.011. PubMed PMID: 23459248; PubMed Central PMCID: PMCPMC3991390.

18. Tsai YC, Du D, Domínguez-Malfavón L, Dimastrogiovanni D, Cross J, Callaghan AJ, et al. Recognition of the 70S ribosome and polysome by the RNA degradosome in *Escherichia coli*. Nucleic Acids Res. 2012;40(20):10417-31. Epub 20120825. doi: 10.1093/nar/gks739. PubMed PMID: 22923520; PubMed Central PMCID: PMCPMC3488216.

19. Leroy A, Vanzo NF, Sousa S, Dreyfus M, Carpousis AJ. Function in *Escherichia coli* of the non-catalytic part of RNase E: role in the degradation of ribosome-free mRNA. Mol Microbiol. 2002;45(5):1231-43. doi: 10.1046/j.1365-2958.2002.03104.x. PubMed PMID: 12207692.

20. Dendooven T, Paris G, Shkumatov AV, Islam MS, Burt A, Kubańska MA, et al. Multi-scale ensemble properties of the *Escherichia coli* RNA degradosome. Mol Microbiol. 2022;117(1):102-20. Epub 20210925. doi: 10.1111/mmi.14800. PubMed PMID: 34415624; PubMed Central PMCID: PMCPMC7613265.

21. Sinha D, De Lay NR. Target recognition by RNase E RNA-binding domain AR2 drives sRNA decay in the absence of PNPase. Proc Natl Acad Sci U S A. 2022;119(48):e2208022119. Epub 20221121. doi: 10.1073/pnas.2208022119. PubMed PMID: 36409892; PubMed Central PMCID: PMCPMC9860253.

22. Lee K, Zhan X, Gao J, Qiu J, Feng Y, Meganathan R, et al. RraA. a protein inhibitor of RNase E activity that globally modulates RNA abundance in *E. coli*. Cell. 2003;114(5):623-34. PubMed PMID: 13678585.

23. Górna MW, Pietras Z, Tsai YC, Callaghan AJ, Hernández H, Robinson CV, Luisi BF. The regulatory protein RraA modulates RNA-binding and helicase activities of the E. coli RNA degradosome. Rna. 2010;16(3):553-62. Epub 20100127. doi: 10.1261/rna.1858010. PubMed PMID: 20106955; PubMed Central PMCID: PMCPMC2822920.

24. Gao J, Lee K, Zhao M, Qiu J, Zhan X, Saxena A, et al. Differential modulation of E. coli mRNA abundance by inhibitory proteins that alter the composition of the degradosome. Mol Microbiol. 2006;61(2):394-406. Epub 20060612. doi: 10.1111/j.1365-2958.2006.05246.x. PubMed PMID: 16771842.

25. Prud'homme-Généreux A, Beran RK, Iost I, Ramey CS, Mackie GA, Simons RW. Physical and functional interactions among RNase E, polynucleotide phosphorylase and the cold-shock protein, CsdA: evidence for a 'cold shock degradosome'. Molecular Microbiology. 2004;54(5):1409-21. doi: https://doi.org/10.1111/j.1365-2958.2004.04360.x.

26. Blum E, Py B, Carpousis AJ, Higgins CF. Polyphosphate kinase is a component of the Escherichia coli RNA degradosome. Molecular Microbiology. 1997;26(2):387-98. doi: https://doi.org/10.1046/j.1365-2958.1997.5901947.x.

27. Kannaiah S, Goldberger O, Alam N, Barnabas G, Pozniak Y, Nussbaum-Shochat A, et al. MinD-RNase E interplay controls localization of polar mRNAs in E. coli. Embo j. 2024;43(4):637-62. Epub 20240119. doi: 10.1038/s44318-023-00026-9. PubMed PMID: 38243117; PubMed Central PMCID: PMCPMC10897333.

28. Taghbalout A, Rothfield L. RNaseE and the other constituents of the RNA degradosome are components of the bacterial cytoskeleton. Proceedings of the National Academy of Sciences. 2007;104(5):1667-72. doi: 10.1073/pnas.0610491104.

29. Ikeda Y, Yagi M, Morita T, Aiba H. Hfq binding at RhlB-recognition region of RNase E is crucial for the rapid degradation of target mRNAs mediated by sRNAs in Escherichia coli. Mol Microbiol. 2011;79(2):419-32. Epub 20101118. doi: 10.1111/j.1365-2958.2010.07454.x. PubMed PMID: 21219461.

30. Ait-Bara S, Carpousis AJ, Quentin Y. RNase E in the gamma-Proteobacteria: conservation of intrinsically disordered noncatalytic region and molecular evolution of microdomains. Mol Genet Genomics. 2015;290(3):847-62. Epub 20141129. doi: 10.1007/s00438-014-0959-5. PubMed PMID: 25432321; PubMed Central PMCID: PMCPMC4435900.

31. Goldblum K, Apririon D. Inactivation of the ribonucleic acid-processing enzyme ribonuclease E blocks cell division. J Bacteriol. 1981;146(1):128-32. doi: 10.1128/jb.146.1.128-132.1981. PubMed PMID: 6163761; PubMed Central PMCID: PMCPMC217061.

32. Bernstein JA, Lin PH, Cohen SN, Lin-Chao S. Global analysis of *Escherichia coli* RNA degradosome function using DNA microarrays. Proc Natl Acad Sci U S A. 2004;101(9):2758-63. Epub 20040223. doi: 10.1073/pnas.0308747101. PubMed PMID: 14981237; PubMed Central PMCID: PMCPMC365694.

847 33. Kido M, Yamanaka K, Mitani T, Niki H, Ogura T, Hiraga S. RNase E polypeptides lacking a
848 carboxyl-terminal half suppress a mukB mutation in *Escherichia coli*. J Bacteriol. 1996;178(13):3917-
849 25. doi: 10.1128/jb.178.13.3917-3925.1996. PubMed PMID: 8682798; PubMed Central PMCID:
850 PMCPMC232654.
851 34. Lopez PJ, Marchand I, Joyce SA, Dreyfus M. The C-terminal half of RNase E, which organizes
852 the *Escherichia coli* degradosome, participates in mRNA degradation but not rRNA processing in vivo.
853 Mol Microbiol. 1999;33(1):188-99. doi: 10.1046/j.1365-2958.1999.01465.x. PubMed PMID:
854 10411735.
855 35. Hardwick SW, Chan VS, Broadhurst RW, Luisi BF. An RNA degradosome assembly in
856 *Caulobacter crescentus*. Nucleic Acids Res. 2011;39(4):1449-59. Epub 20101015. doi:
857 10.1093/nar/gkq928. PubMed PMID: 20952404; PubMed Central PMCID: PMCPMC3045602.
858 36. Voss JE, Luisi BF, Hardwick SW. Molecular recognition of RhlB and RNase D in the
859 *Caulobacter crescentus* RNA degradosome. Nucleic Acids Res. 2014;42(21):13294-305. Epub
860 20141111. doi: 10.1093/nar/gku1134. PubMed PMID: 25389270; PubMed Central PMCID:
861 PMCPMC4245959.
862 37. Zhang JY, Deng XM, Li FP, Wang L, Huang QY, Zhang CC, Chen WL. RNase E forms a
863 complex with polynucleotide phosphorylase in cyanobacteria via a cyanobacterial-specific nonapeptide
864 in the noncatalytic region. RNA. 2014;20(4):568-79. Epub 20140221. doi: 10.1261/rna.043513.113.
865 PubMed PMID: 24563514; PubMed Central PMCID: PMCPMC3964918.
866 38. Yan HD, Qin XX, Wang L, Chen WL. Both Enolase and the DEAD-Box RNA Helicase CrhB
867 Can Form Complexes with RNase E in *Anabaena* sp. Strain PCC 7120. Applied and environmental
868 microbiology. 2020;86(13). doi: 10.1128/AEM.00425-20. PubMed PMID: WOS:000546650600011.
869 39. Zhou C, Zhang JY, Hu XY, Li CC, Wang L, Huang QY, Chen WL. RNase II binds to RNase E
870 and modulates its endoribonucleolytic activity in the cyanobacterium *Anabaena* PCC 7120. Nuceic
871 Acid Res. 2020;48(7):3922-34. doi: 10.1093/nar/gkaa092. PubMed PMID: WOS:000525957700040.
872 40. Purusharth RI, Klein F, Sulthana S, Jäger S, Jagannadham MV, Evguenieva-Hackenberg E, et
873 al. Exoribonuclease R Interacts with Endoribonuclease E and an RNA Helicase in the Psychrotrophic
874 Bacterium Pseudomonas syringae Lz4W*. Journal of Biological Chemistry. 2005;280(15):14572-8.
875 doi: https://doi.org/10.1074/jbc.M413507200.
876 41. Jäger S, Fuhrmann O, Heck C, Hebermehl M, Schiltz E, Rauhut R, Klug G. An mRNA
877 degrading complex in *Rhodobacter capsulatus*. Nucleic Acids Res. 2001;29(22):4581-8. doi:
878 10.1093/nar/29.22.4581. PubMed PMID: 11713307; PubMed Central PMCID: PMCPMC92556.
879 42. Aït-Bara S, Carpousis Agamemnon J. Characterization of the RNA Degradosome of
880 *Pseudoalteromonas haloplanktis*: Conservation of the RNase E-RhlB Interaction in the
881 Gammaproteobacteria. Journal of Bacteriology. 2010;192(20):5413-23. doi: 10.1128/jb.00592-10.

882 43. Hardwick SW, Gubbey T, Hug I, Jenal U, Luisi BF. Crystal structure of *Caulobacter crescentus*
883 polynucleotide phosphorylase reveals a mechanism of RNA substrate channelling and RNA
884 degradosome assembly. Open Biology. 2012;2(4):120028. doi: 10.1098/rsob.120028.
885 44. Nurmohamed S, Vaidialingam B, Callaghan AJ, Luisi BF. Crystal Structure of Escherichia coli
886 Polynucleotide Phosphorylase Core Bound to RNase E, RNA and Manganese: Implications for
887 Catalytic Mechanism and RNA Degradosome Assembly. Journal of Molecular Biology.
888 2009;389(1):17-33. doi: https://doi.org/10.1016/j.jmb.2009.03.051.
889 45. Green SK, Schroth MN, Cho JJ, Kominos SK, Vitanza-jack VB. Agricultural plants and soil as
890 a reservoir for *Pseudomonas aeruginosa*. Applied microbiology. 1974;28(6):987-91. Epub 1974/12/01.
891 PubMed PMID: 4217591; PubMed Central PMCID: PMCPMC186868.
892 46. Hardalo C, Edberg SC. *Pseudomonas aeruginosa*: assessment of risk from drinking water.
893 Critical reviews in microbiology. 1997;23(1):47-75. Epub 1997/01/01. doi:
894 10.3109/10408419709115130. PubMed PMID: 9097014.
895 47. Pendleton JN, Gorman SP, Gilmore BF. Clinical relevance of the ESKAPE pathogens. Expert
896 review of anti-infective therapy. 2013;11(3):297-308. Epub 2013/03/06. doi: 10.1586/eri.13.12.
897 PubMed PMID: 23458769.
898 48. https://www.who.int/news/item/27-02-2017-who-publishes-list-of-bacteria-for-which-new-
899 antibiotics-are-urgently-needed.
900 49. Garcia-Clemente M, de la Rosa D, Máiz L, Girón R, Blanco M, Olveira C, et al. Impact of
901 Pseudomonas aeruginosa Infection on Patients with Chronic Inflammatory Airway Diseases. Journal of
902 clinical medicine. 2020;9(12). Epub 2020/12/02. doi: 10.3390/jcm9123800. PubMed PMID: 33255354.
903 50. Urwin L, Okurowska K, Crowther G, Roy S, Garg P, Karunakaran E, et al. Corneal Infection
904 Models: Tools to Investigate the Role of Biofilms in Bacterial Keratitis. Cells. 2020;9(11). Epub
905 2020/11/14. doi: 10.3390/cells9112450. PubMed PMID: 33182687; PubMed Central PMCID:
906 PMCPMC7696224.
907 51. Costerton JW, Stewart PS, Greenberg EP. Bacterial biofilms: a common cause of persistent
908 infections. Science (New York, NY). 1999;284(5418):1318-22. Epub 1999/05/21. doi:
909 10.1126/science.284.5418.1318. PubMed PMID: 10334980.
910 52. Lu Q, Eggimann P, Luyt CE, Wolff M, Tamm M, François B, et al. Pseudomonas aeruginosa
911 serotypes in nosocomial pneumonia: prevalence and clinical outcomes. Critical care (London, England).
912 2014;18(1):R17. Epub 2014/01/17. doi: 10.1186/cc13697. PubMed PMID: 24428878; PubMed Central
913 PMCID: PMCPMC4057348.
914 53. Hancock RE. Resistance mechanisms in *Pseudomonas aeruginosa* and other nonfermentative
915 gram-negative bacteria. Clin Infect Dis. 1998;27 Suppl 1:S93-9. Epub 1998/08/26. PubMed PMID:
916 9710677.
917 54. Van den Bossche A, Hardwick SW, Ceyssens PJ, Hendrix H, Voet M, Dendooven T, et al.
918 Structural elucidation of a novel mechanism for the bacteriophage-based inhibition of the RNA

919 degradosome. Elife. 2016;5. Epub 20160722. doi: 10.7554/eLife.16413. PubMed PMID: 27447594;
920 PubMed Central PMCID: PMCPMC4980113.
921 55. Hausmann S, Gonzalez D, Geiser J, Valentini M. The DEAD-box RNA helicase RhlE2 is a
922 global regulator of *Pseudomonas aeruginosa* lifestyle and pathogenesis. Nucleic Acids Res.
923 2021;49(12):6925-40. doi: 10.1093/nar/gkab503. PubMed PMID: 34151378; PubMed Central PMCID:
924 PMCPMC8266600.
925 56. Hausmann S, Geiser J, Allen GE, Geslain SAM, Valentini M. Intrinsically disordered regions
926 regulate RhlE RNA helicase functions in bacteria. Nucleic Acids Res. 2024. Epub 20240614. doi:
927 10.1093/nar/gkae511. PubMed PMID: 38874491.
928 57. Sonnleitner E, Romeo A, Bläsi U. Small regulatory RNAs in *Pseudomonas aeruginosa*. RNA
929 Biol. 2012;9(4):364-71. Epub 2012/02/18. doi: 10.4161/rna.19231. PubMed PMID: 22336763.
930 58. Valentini M, Gonzalez D, Mavridou DA, Filloux A. Lifestyle transitions and adaptive
931 pathogenesis of *Pseudomonas aeruginosa*. Current opinion in microbiology. 2018;41:15-20. Epub
932 2017/11/23. doi: 10.1016/j.mib.2017.11.006. PubMed PMID: 29166621.
933 59. Nishio S-y, Itoh T. Arginine-rich RNA binding domain and protein scaffold domain of RNase
934 E are important for degradation of RNAI but not for that of the Rep mRNA of the ColE2 plasmid.
935 Plasmid. 2009;62(2):83-7. doi: https://doi.org/10.1016/j.plasmid.2009.04.002.
936 60. Hamouche L, Poljak L, Carpousis AJ. Polyribosome-Dependent Clustering of Membrane-
937 Anchored RNA Degradosomes To Form Sites of mRNA Degradation in *Escherichia coli*. mBio.
938 2021;12(5):e0193221. Epub 20210907. doi: 10.1128/mBio.01932-21. PubMed PMID: 34488454;
939 PubMed Central PMCID: PMCPMC8546579.
940 61. Al-Husini N, Tomares DT, Bitar O, Childers WS, Schrader JM. α-Proteobacterial RNA
941 Degradosomes Assemble Liquid-Liquid Phase-Separated RNP Bodies. Mol Cell. 2018;71(6):1027-
942 39.e14. Epub 20180906. doi: 10.1016/j.molcel.2018.08.003. PubMed PMID: 30197298; PubMed
943 Central PMCID: PMCPMC6151146.
944 62. Khemici V, Poljak L, Luisi BF, Carpousis AJ. The RNase E of *Escherichia coli* is a membrane-
945 binding protein. Mol Microbiol. 2008;70(4):799-813. Epub 20081002. doi: 10.1111/j.1365-
946 2958.2008.06454.x. PubMed PMID: 18976283; PubMed Central PMCID: PMCPMC7610891.
947 63. Schuck A, Diwa A, Belasco JG. RNase E autoregulates its synthesis in Escherichia coli by
948 binding directly to a stem-loop in the rne 5' untranslated region. Mol Microbiol. 2009;72(2):470-8. Epub
949 20090306. doi: 10.1111/j.1365-2958.2009.06662.x. PubMed PMID: 19320830; PubMed Central
950 PMCID: PMCPMC2857391.
951 64. Liu S-J, Lin G-M, Yuan Y-Q, Chen W, Zhang J-Y, Zhang C-C. A conserved protein inhibitor
952 brings under check the activity of RNase E in cyanobacteria. Nucleic Acids Research. 2024;52(1):404-
953 19. doi: 10.1093/nar/gkad1094.

65. Karimova G, Ullmann A, Ladant D. [5] A bacterial two-hybrid system that exploits a cAMP signaling cascade in Escherichia coli. In: Thorner J, Emr SD, Abelson JN, editors. Methods in Enzymology. 328: Academic Press; 2000. p. 59-73.

66. Jander G, Rahme Laurence G, Ausubel Frederick M. Positive Correlation between Virulence ofPseudomonas aeruginosa Mutants in Mice and Insects. Journal of Bacteriology. 2000;182(13):3843-5. doi: 10.1128/jb.182.13.3843-3845.2000.

67. Lin J, Cheng J, Wang Y, Shen X. The Pseudomonas Quinolone Signal (PQS): Not Just for Quorum Sensing Anymore. Front Cell Infect Microbiol. 2018;8:230. Epub 20180704. doi: 10.3389/fcimb.2018.00230. PubMed PMID: 30023354; PubMed Central PMCID: PMCPMC6039570.

68. Gonçalves T, Vasconcelos U. Colour Me Blue: The History and the Biotechnological Potential of Pyocyanin. Molecules. 2021;26(4). Epub 20210210. doi: 10.3390/molecules26040927. PubMed PMID: 33578646; PubMed Central PMCID: PMCPMC7916356.

69. Chou HT, Li J-Y, Lu C-D. Functional Characterization of the agtABCD and agtSR Operons for 4-Aminobutyrate and 5-Aminovalerate Uptake and Regulation in Pseudomonas aeruginosa PAO1. Current Microbiology. 2014;68(1):59-63. doi: 10.1007/s00284-013-0446-y.

70. Hauser AR. The type III secretion system of Pseudomonas aeruginosa: infection by injection. Nat Rev Microbiol. 2009;7(9):654-65. doi: 10.1038/nrmicro2199. PubMed PMID: 19680249; PubMed Central PMCID: PMCPMC2766515.

71. Nandana V, Al-Husini N, Vaishnav A, Dilrangi KH, Schrader JM. Caulobacter crescentus RNase E condensation contributes to autoregulation and fitness. Mol Biol Cell. 2024;35(8):ar104. Epub 20240612. doi: 10.1091/mbc.E23-12-0493. PubMed PMID: 38865176; PubMed Central PMCID: PMCPMC11321048.

72. Wurtzel O, Yoder-Himes DR, Han K, Dandekar AA, Edelheit S, Greenberg EP, et al. The single-nucleotide resolution transcriptome of Pseudomonas aeruginosa grown in body temperature. PLoS Pathog. 2012;8(9):e1002945. Epub 20120927. doi: 10.1371/journal.ppat.1002945. PubMed PMID: 23028334; PubMed Central PMCID: PMCPMC3460626.

73. de Araújo Hugo L, Picinato Beatriz A, Lorenzetti Alan PR, Muthunayake Nisansala S, Rathnayaka-Mudiyanselage IW, dos Santos Naara M, et al. The DEAD-box RNA helicase RhlB is required for efficient RNA processing at low temperature in Caulobacter. Microbiology Spectrum. 2023;11(6):e01934-23. doi: 10.1128/spectrum.01934-23.

74. Vaillancourt M, Galdino ACM, Limsuwannarot SP, Celedonio D, Dimitrova E, Broerman M, et al. A compensatory RNase E variation increases Iron Piracy and Virulence in multidrug-resistant *Pseudomonas aeruginosa* during Macrophage infection. PLoS Pathog. 2023;19(4):e1010942. Epub 20230407. doi: 10.1371/journal.ppat.1010942. PubMed PMID: 37027441; PubMed Central PMCID: PMCPMC10115287.

989 75. Khemici V, Toesca I, Poljak L, Vanzo NF, Carpousis AJ. The RNase E of *Escherichia coli* has
990 at least two binding sites for DEAD-box RNA helicases: functional replacement of RhlB by RhlE.
991 Molecular Microbiology. 2004;54(5):1422-30. doi: https://doi.org/10.1111/j.1365-2958.2004.04361.x.
992 76. Worrall JA, Howe FS, McKay AR, Robinson CV, Luisi BF. Allosteric activation of the ATPase
993 activity of the *Escherichia coli* RhlB RNA helicase. J Biol Chem. 2008;283(9):5567-76. PubMed
994 PMID: 18165229.
995 77. Lüthi E, Mercenier A, Haas D. The arcABC Operon Required for Fermentative Growth of
996 Pseudomonas aeruginosa on Arginine: Tn5-751-assisted Cloning and Localization of Structural Genes.
997 Microbiology. 1986;132(10):2667-75. doi: https://doi.org/10.1099/00221287-132-10-2667.
998 78. Gamper M, Ganter B, Polito MR, Haas D. RNA processing modulates the expression of the
999 *arcDABC* operon in *Pseudomonas aeruginosa*. Journal of Molecular Biology. 1992;226(4):943-57. doi:
1000 https://doi.org/10.1016/0022-2836(92)91044-P.
1001 79. Rietsch A, Vallet-Gely I, Dove SL, Mekalanos JJ. ExsE, a secreted regulator of type III
1002 secretion genes in Pseudomonas aeruginosa. Proc Natl Acad Sci U S A. 2005;102(22):8006-11. Epub
1003 20050523. doi: 10.1073/pnas.0503005102. PubMed PMID: 15911752; PubMed Central PMCID:
1004 PMCPMC1142391.
1005 80. Laville J, Voisard C, Keel C, Maurhofer M, Défago G, Haas D. Global control in Pseudomonas
1006 fluorescens mediating antibiotic synthesis and suppression of black root rot of tobacco. Proc Natl Acad
1007 Sci U S A. 1992;89(5):1562-6. doi: 10.1073/pnas.89.5.1562. PubMed PMID: 1311842; PubMed Central
1008 PMCID: PMCPMC48492.
1009 81. Ye RW, Haas D, Ka JO, Krishnapillai V, Zimmermann A, Baird C, Tiedje JM. Anaerobic
1010 activation of the entire denitrification pathway in Pseudomonas aeruginosa requires Anr, an analog of
1011 Fnr. J Bacteriol. 1995;177(12):3606-9. doi: 10.1128/jb.177.12.3606-3609.1995. PubMed PMID:
1012 7768875; PubMed Central PMCID: PMCPMC177071.
1013 82. Altschul SF, Gish W, Miller W, Myers EW, Lipman DJ. Basic local alignment search tool. J
1014 Mol Biol. 1990;215(3):403-10. doi: 10.1016/s0022-2836(05)80360-2. PubMed PMID: 2231712.
1015 83. Pagès HA, P.; Gentleman, R.; DebRoy, S. Biostrings: Efficient manipulation of biological
1016 strings. 2024.
1017 84. Grant BJ, Rodrigues AP, ElSawy KM, McCammon JA, Caves LS. Bio3d: an R package for the
1018 comparative analysis of protein structures. Bioinformatics. 2006;22(21):2695-6. Epub 20060829. doi:
1019 10.1093/bioinformatics/btl461. PubMed PMID: 16940322.
1020 85. Edgar RC. MUSCLE: multiple sequence alignment with high accuracy and high throughput.
1021 Nucleic Acids Res. 2004;32(5):1792-7. Epub 20040319. doi: 10.1093/nar/gkh340. PubMed PMID:
1022 15034147; PubMed Central PMCID: PMCPMC390337.
1023 86. Ream JA, Lewis LK, Lewis KA. Rapid agarose gel electrophoretic mobility shift assay for
1024 quantitating protein: RNA interactions. Anal Biochem. 2016;511:36-41. Epub 20160802. doi:
1025 10.1016/j.ab.2016.07.027. PubMed PMID: 27495142; PubMed Central PMCID: PMCPMC5002362.

87. Schindelin J, Arganda-Carreras I, Frise E, Kaynig V, Longair M, Pietzsch T, et al. Fiji: an open-source platform for biological-image analysis. Nat Methods. 2012;9(7):676-82. Epub 20120628. doi: 10.1038/nmeth.2019. PubMed PMID: 22743772; PubMed Central PMCID: PMCPMC3855844.

88. Team RC. R: A Language and Environment for Statistical Computing. R Foundation for Statistical Computing. Vienna, Austria2023.

89. Bordi C, Lamy MC, Ventre I, Termine E, Hachani A, Fillet S, et al. Regulatory RNAs and the HptB/RetS signalling pathways fine-tune Pseudomonas aeruginosa pathogenesis. Mol Microbiol. 2010;76(6):1427-43. Epub 20100401. doi: 10.1111/j.1365-2958.2010.07146.x. PubMed PMID: 20398205; PubMed Central PMCID: PMCPMC2904497.

90. Langmead B, Salzberg SL. Fast gapped-read alignment with Bowtie 2. Nature Methods. 2012;9(4):357-9. doi: 10.1038/nmeth.1923.

91. Lawrence M, Huber W, Pagès H, Aboyoun P, Carlson M, Gentleman R, et al. Software for Computing and Annotating Genomic Ranges. PLOS Computational Biology. 2013;9(8):e1003118. doi: 10.1371/journal.pcbi.1003118.

92. Love MI, Huber W, Anders S. Moderated estimation of fold change and dispersion for RNA-seq data with DESeq2. Genome Biology. 2014;15(12):550. doi: 10.1186/s13059-014-0550-8.

93. B. TDM. KEGGREST: Client-side REST access to the Kyoto Encyclopedia of Genes and Genomes (KEGG). doi:10.18129/B9.bioc.KEGGREST. R package version 1420, https://bioconductororg/packages/KEGGREST2023.

94. de Araújo HL, Picinato BA, Lorenzetti APR, Muthunayake NS, Rathnayaka-Mudiyanselage IW, Dos Santos NM, et al. The DEAD-box RNA helicase RhlB is required for efficient RNA processing at low temperature in Caulobacter. Microbiol Spectr. 2023:e0193423. Epub 2023/10/18. doi: 10.1128/spectrum.01934-23. PubMed PMID: 37850787.

95. Erdős G, Pajkos M, Dosztányi Z. IUPred3: prediction of protein disorder enhanced with unambiguous experimental annotation and visualization of evolutionary conservation. Nucleic Acids Research. 2021;49(W1):W297-W303. doi: 10.1093/nar/gkab408.

96. Xue B, Dunbrack RL, Williams RW, Dunker AK, Uversky VN. PONDR-FIT: a meta-predictor of intrinsically disordered amino acids. Biochim Biophys Acta. 2010;1804(4):996-1010. Epub 20100125. doi: 10.1016/j.bbapap.2010.01.011. PubMed PMID: 20100603; PubMed Central PMCID: PMCPMC2882806.

97. McLaren RS, Newbury SF, Dance GS, Causton HC, Higgins CF. mRNA degradation by processive 3'-5' exoribonucleases in vitro and the implications for prokaryotic mRNA decay in vivo. J Mol Biol. 1991;221(1):81-95. PubMed PMID: 1920421.

98. Bolte S, Cordelières FP. A guided tour into subcellular colocalization analysis in light microscopy. J Microsc. 2006;224(Pt 3):213-32. doi: 10.1111/j.1365-2818.2006.01706.x. PubMed PMID: 17210054.

1063 **Figure Legends**

1064

1065 **Figure 1: Comparison of *E. coli* (Ec) and *P. aeruginosa* (Pa) RNase E architecture. (A)** Ec RNase
1066 E architecture, adapted from [17]. The NTD is shown is grey, and experimentally defined regions
1067 necessary for interaction with the membrane, with RNA, or with the three core protein partners are
1068 highlighted in red, dark blue, and yellow/purple/pink, respectively. **(B)** Pa RNase E architecture based
1069 on in-silico analyses performed in Fig S1-S2 and in [30]. The SLiM nomenclature was taken from [30],
1070 while the consensus sequence characterising each SLiM was specifically adapted based on sequence
1071 conservation within the Pseudomonas genus (Fig S1). MTS: membrane-targeting sequence, AR4:
1072 arginine-rich motif 4, REER-repeats: region with high frequency of occurrence of "RE[E/D]R" motif,
1073 M29: motif 29, AR1: arginine-rich motif 1, M20: motif 20, NDPR: motif with a highly conserved NDPR
1074 sequence. All diagrams were drawn to scale. IUPRED3 [95] and PONDR [96] predictions of disorder
1075 propensity (probability score) are shown for Ec RNase E **(A)** and Pa RNase E **(B)**.

1076

1077 **Figure 2: RNA binding of Pa RNase E CTD via the AR1, AR4, and REER SLiMs. (A)** EMSA with
1078 purified His-Smt3 tagged RNase E CTD$^{572-1057}$ variants having either the native sequence (WT) or
1079 systematic alanine mutation of the arginine residues found within the REER-repeats region (REERmut),
1080 the AR4 SLiM (AR4mut) or the AR1 SLiM (AR1mut). The *malEF* mRNA intergenic region was used
1081 as a substrate [97]. Ratios of RNA:protein ranging from 1:10 to 1:80 were tested. See Fig S2 for
1082 additional EMSA with additional RNA:protein ratios. **(B)** Representative microscopy images of a PAO1
1083 strain expressing the RNase E-msfGFP fusion or mutated or truncated variants as indicated. **(C)**
1084 Quantification of signal intensity variance in the strains of panel B as indication of foci disappearance
1085 (see methods). **(D)** Representative microscopy images of a PAO1 strain expressing the RNase E-
1086 msfGFP fusion after exposure to rifampicin (+ Rif, exposure to a concentration of 100 µg/mL for 30
1087 minutes) or to DMSO as a negative control (- Rif). Corrected mean fluorescent signal intensity **(E)** and
1088 signal intensity variance **(F)** is showed in the graphs (see methods). Each quantification analysis
1089 involved at least 50 individual cells. The scale is 2 µm. Statistical significance was assessed by

1090 performing t-tests using R. p-values for comparisons tested are indicated as follows: *:<0.05; **:<0.01;
1091 ***:<0.001; ****:<0.0001.
1092
1093 **Figure 3**: **Identification of scaffold domain-dependent RNase E protein partners by pull-down**
1094 **assays and mapping of the interactions by bacterial two-hybrid assays (A)** Volcano plot
1095 highlighting the relative enrichment of proteins co-eluting with the RNase E^{1-1057}-Strep bait protein
1096 compared to the untagged negative control. The plot was generated from the average peptide count
1097 obtained in duplicate pull-down experiments. An arbitrary threshold of 5.5-fold change was chosen for
1098 selection of candidate (c) proteins. **(B)** Scatterplot highlighting comparative enrichment of proteins co-
1099 eluting with the RNase E^{1-1057}-Strep bait protein (x axis) or with the RNase E^{1-529}-Strep bait protein (y
1100 axis) compared to the untagged negative control. **(C)** Quantification of β-galactosidase activity in *E.*
1101 *coli* BTH101 cells co-expressing T18-RNase E with T25-PNPase, T25-RhlB, T25-ArcB, T25-GdhB or
1102 T25-RpoB. Interaction between T18-RNase E and a T25-tagged protein partner results in a significant
1103 restoration of β-galactosidase activity compared with empty vector (e.v.) negative controls. Unpaired
1104 Welch's t-tests was performed using GraphPad Prism to assess differences between every tested protein-
1105 protein interaction and the respective negative control. ***: p-value <0.0001; n.s: not significant (99%
1106 confidence level). **(D-F)** Mapping of the interaction between RNase E and PNPase **(D)**, RhlB **(E)**, or
1107 ArcB **(F)** by quantification of β-galactosidase activity in *E. coli* BTH101 cells co-expressing T25-
1108 PNPase **(D)**, T25-RhlB **(E)**, or T25-ArcB **(F)** and either T18-RNase E or one of eight to ten truncated
1109 T18-RNase E fragments. Empty vector (e.v.) negative controls are included into each separate graph
1110 for comparison.
1111
1112 **Figure 4: PNPase and RhlB directly interact with RNase E scaffold domain via NDPR and AR1**
1113 **SLiMs, respectively.** Purified Flag-tagged RNase E^{1-529} or RNase $E^{572-1057}$ proteins having either native
1114 or mutated sequence were used as baits, immobilized to anti-flag magnetic beads and incubated with
1115 purified His-Smt3 tagged PNPase **(A)** or RhlB **(B)** proteins to assess direct protein binding. I: input, F:
1116 free fraction, B: bound fraction. NDPRmut, AR1mut: mutations of NDPR and AR1 SLiMs, respectively
1117 (see Table S4). Binding assays were repeated at least 2 times and representative gels are shown.

1118

1119 **Figure 5**: **Colocalisation of PNPase or RhlB with RNase E foci is dependent on their interaction**
1120 **with NDPR and AR1 RNase E SLiMs, respectively. (A)** Visualisation of PNPase-msfGFP (upper
1121 panels) or RhlB-msfGFP (lower panels) fusion and RNase E-mCherry fusion co-expressed in the same
1122 strain. Pearson's and M coefficients were calculated in Fiji using the JaCoP plugin [98]. Three
1123 independent images were used, each containing at least 30 cells, and an average coefficient was
1124 calculated from the three values obtained with each image. **(B)** Visualisation of PNPase-msfGFP (upper
1125 panels) and RhlB-msfGFP (lower panels) in strains expressing either the native RNase E protein (full
1126 length) or truncated variants, as indicated above each image. Scale is 2 µm.

1127

1128 **Figure 6: Phenotypes affected by deletion or mutation of RNase E scaffolding domain. (A)** Growth
1129 on NA agar plates at 37°C or 16°C, or under low vs high pH conditions of wild-type (WT), *rne588*,
1130 *rne529*, *rne*AR1^{mut}, *rne*NDPR^{mut}, and *rne*AR1+AR4+REER^{mut} strains, as indicated. Experiments were
1131 performed in biological independent triplicates; a representative plate is shown. **(B)** Measured colony
1132 size for the different mutant strains as indicated. Quantification was done using the Measure function
1133 in Image J after drawing a circle around the edge of each colony. 11 to 13 colonies were quantified for
1134 each strain. A one-way Anova test was performed using GraphPad and comparing the colony size of
1135 each mutant strain to that of the WT strain. ***: p-value <0.0001; n.s: not significant (99% confidence
1136 interval). **(C)** Growth in NYB broth at 37°C in 96-well plates of wild-type (WT), *rne588*, *rne529*,
1137 *rne*AR1^{mut}, *rne*NDPR^{mut}, and *rne*AR1+AR4+REER^{mut} strains, as indicated. Independent biological
1138 triplicates, each with four technical replicates, were used to generate the average growth curve shown.
1139 **(D)** Killing curves of *G. mellonella* larvae injected with 10 µL of WT or mutant *P. aeruginosa* strains
1140 (as in panel A). The control group was injected with 10 µL of sterile PBS instead. Larvae were incubated
1141 at 37°C and larval death was monitored over 13-26 hours post-injection. A larva was considered dead
1142 when it completely stopped responding to repeated touching stimuli. Two independent replicates were
1143 performed using a total of at least 50 larvae for each strain tested. A Kaplan-Meier test for survival
1144 analysis was performed using GraphPad Prism and comparing the survival curve of each mutant strain
1145 to that of the WT strain. ***: p-value <0.0001; n.s: not significant (99% confidence interval).

1146

1147 **Figure 7: RNA-seq analysis of RNase E CTD truncated mutants reveals broad transcriptome**
1148 **changes. (A-B)** Volcano plots highlighting genes differentially regulated in the **(A)** *rne*$^{1-529}$ (R529) or
1149 **(B)** *rne* $^{1-588}$ (R588) mutant strains compared with the WT strain. Genes significantly up- or down-
1150 regulated (adjusted p-value < 0.05, fold change |FC| ≥ 2) are highlighted in red or blue, respectively.
1151 **(C)** Scatterplot of genes differentially regulated in *rne* $^{1-529}$ strain versus genes differentially regulated
1152 in *rne*$^{1-588}$ strain, highlighting commonalities and differences between the two mutant strains. **(D-E)**
1153 Clustered heat maps of type 3 secretion system **(D)** or ribosomal proteins **(E)** transcript levels in the
1154 RNase E$^{1-529}$ and by about 2-fold in the RNase E$^{1-588}$ strains as compared to the WT strain (fold change).
1155 **(F)** Differential analyses (log 2-fold change) of normalized total reads counts corresponding to the 5'
1156 UTR region of the PA2976 (*rne*) transcript or RNase E NTD coding sequence in the RNase E$^{1-529}$ and
1157 by about 2-fold in the RNase E$^{1-588}$ strains as compared to the WT strain. **(G)** Proportion of loci with 5'
1158 read ends (sequenced fragments) counted only in a strain (numerator) relative to the 5' read ends counted
1159 in that strain and in a WT replica (denominator). A total of 8 million reads was analysed in each strain
1160 to exclude an effect due to the library depth (see methods). Histograms of individual values calculated
1161 per each strain and replicate is shown in Figure S10.

1162

1163 **Figure 8: Model of RNA degradosome in *P. aeruginosa*.** Numbers corresponds to RNase E SLiM
1164 start-end residues involved in membrane, RNA, RhlB or PNPase interaction. RNA is represented as a
1165 dotted line. See discussion for details.

Figure 1

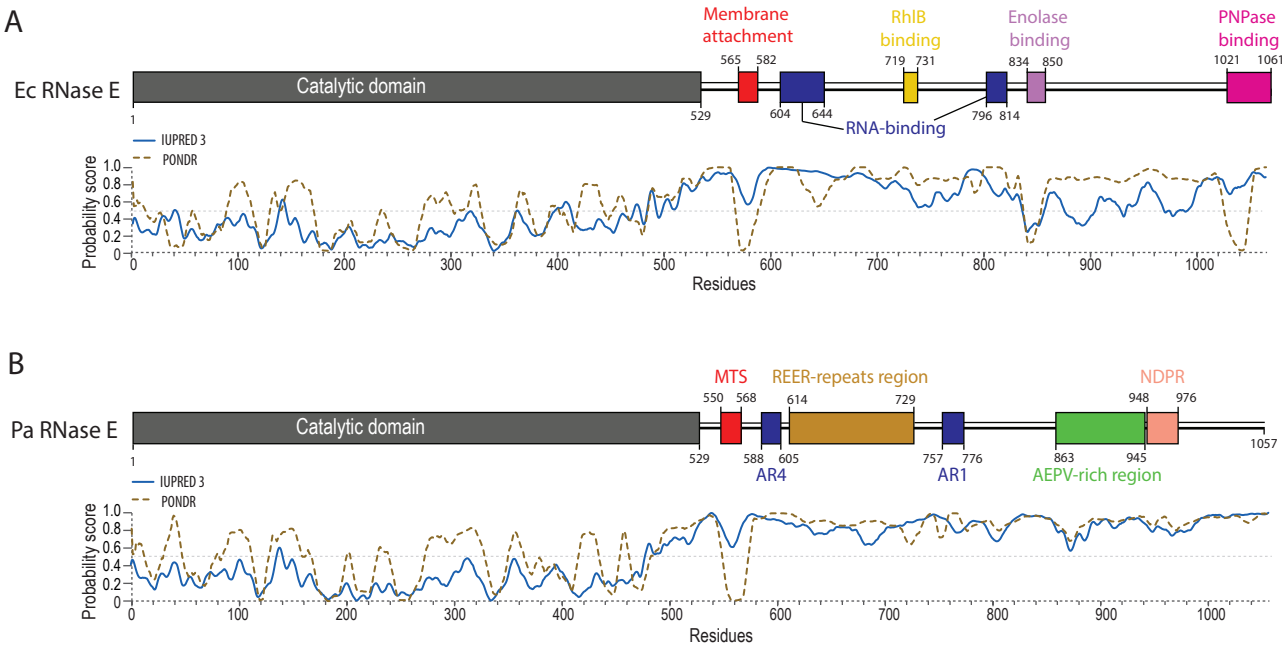
A
Ec RNase E
Catalytic domain
Membrane attachment
565
582
RhlB binding
719
731
Enolase binding
834
850
PNPase binding
1021
1061
1
529
604
644
RNA-binding
796
814
IUPRED 3
PONDR
Probability score
1.0
0.8
0.6
0.4
0.2
0
0
100
200
300
400
500
600
700
800
900
1000
Residues
B
Pa RNase E
Catalytic domain
MTS
550
568
REER-repeats region
614
729
NDPR
948
976
1
529
588
605
AR4
757
776
AR1
863
945
AEPV-rich region
1057
IUPRED 3
PONDR
Probability score
1.0
0.8
0.6
0.4
0.2
0
0
100
200
300
400
500
600
700
800
900
1000
Residues

Figure 2

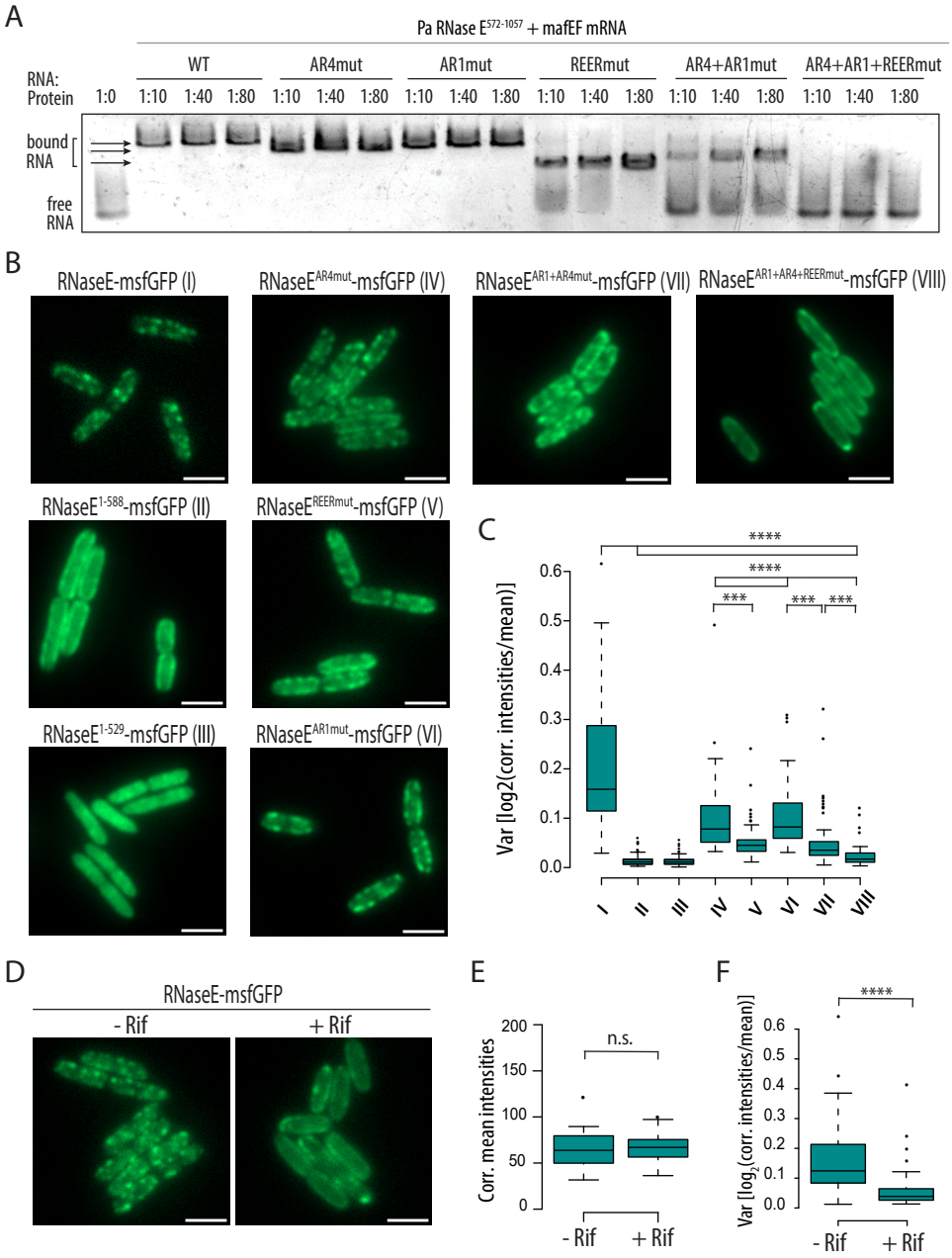
A
Pa RNase E572-1057 + mafEF mRNA
WT
AR4mut
AR1mut
REERmut
AR4+AR1mut
AR4+AR1+REERmut
RNA: Protein
1:0
1:10 1:40 1:80
bound RNA
free RNA
B
RNaseE-msfGFP (I)
RNaseEAR4mut-msfGFP (IV)
RNaseEAR1+AR4mut-msfGFP (VII)
RNaseEAR1+AR4+REERmut-msfGFP (VIII)
RNaseE1-588-msfGFP (II)
RNaseEREERmut-msfGFP (V)
RNaseE1-529-msfGFP (III)
RNaseEAR1mut-msfGFP (VI)
C
Var [log2(corr. intensities/mean)]
0.0
0.1
0.2
0.3
0.4
0.5
0.6
****
***
I
II
III
IV
V
VI
VII
VIII
D
RNaseE-msfGFP
- Rif
+ Rif
E
Corr. mean intensities
0
50
100
150
200
n.s.
- Rif
+ Rif
F
Var [log2(corr. intensities/mean)]
0.0
0.1
0.2
0.3
0.4
0.5
0.6
****
- Rif
+ Rif

Figure 3

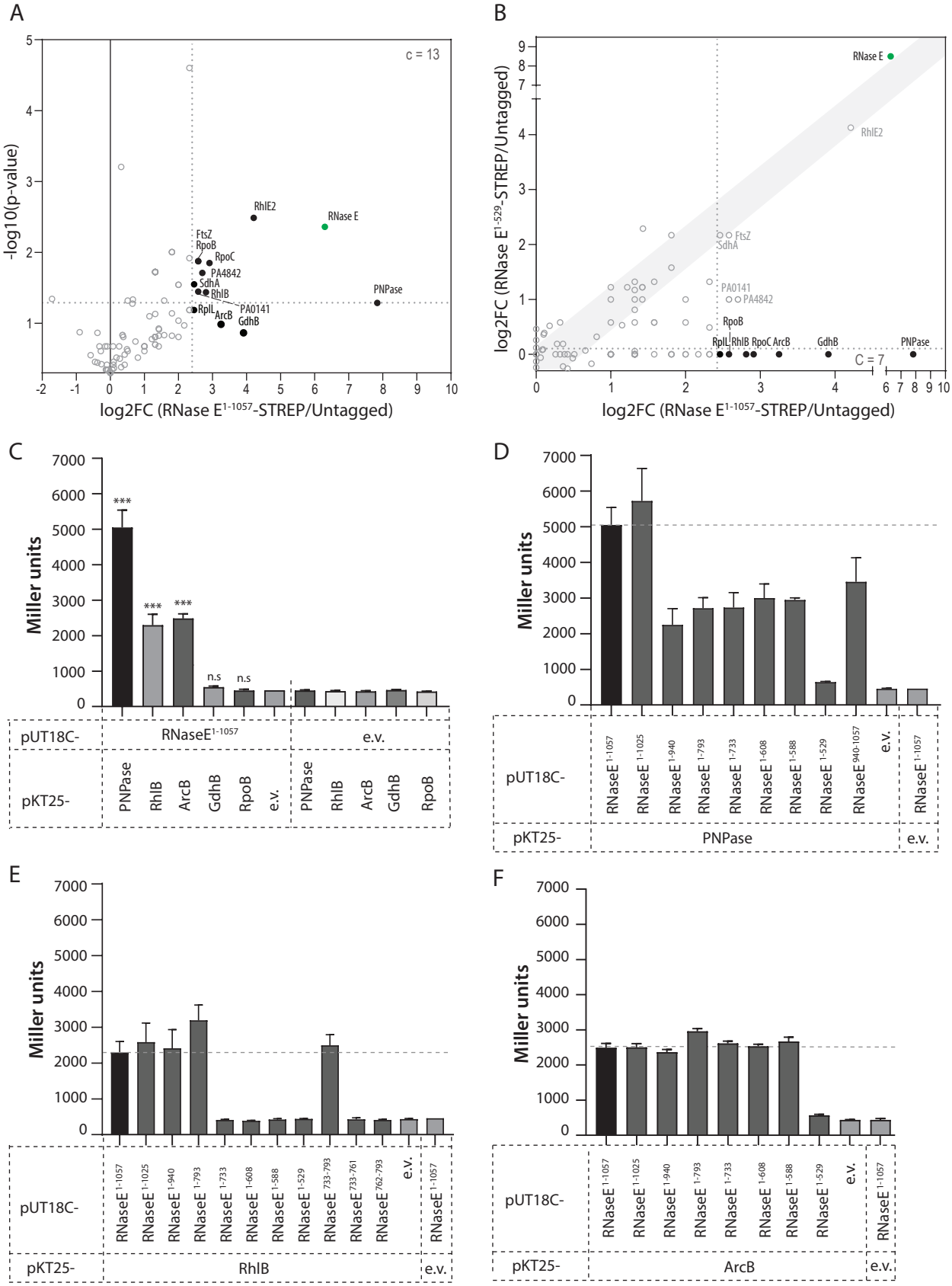
A
c = 13
-log10(p-value)
log2FC (RNase E1-1057-STREP/Untagged)
RhlE2
RNase E
FtsZ
RpoB
RpoC
PA4842
SdhA
RhlB
RplL
ArcB
PA0141
GdhB
PNPase
B
RNase E
RhlE2
FtsZ
SdhA
PA0141
PA4842
RpoB
RplL
RhlB
RpoC
ArcB
GdhB
PNPase
C = 7
log2FC (RNase E1-529-STREP/Untagged)
log2FC (RNase E1-1057-STREP/Untagged)
C
Miller units
***
n.s
pUT18C-
RNaseE1-1057
e.v.
pKT25-
PNPase
RhlB
ArcB
GdhB
RpoB
e.v.
D
Miller units
pUT18C-
RNaseE1-1057
RNaseE1-1025
RNaseE1-940
RNaseE1-793
RNaseE1-733
RNaseE1-608
RNaseE1-588
RNaseE1-529
RNaseE940-1057
e.v.
pKT25-
PNPase
e.v.
E
Miller units
pUT18C-
RNaseE1-1057
RNaseE1-1025
RNaseE1-940
RNaseE1-793
RNaseE1-733
RNaseE1-608
RNaseE1-588
RNaseE1-529
RNaseE733-793
RNaseE733-761
RNaseE762-793
e.v.
pKT25-
RhlB
e.v.
F
Miller units
pUT18C-
RNaseE1-1057
RNaseE1-1025
RNaseE1-940
RNaseE1-793
RNaseE1-733
RNaseE1-608
RNaseE1-588
RNaseE1-529
e.v.
pKT25-
ArcB
e.v.

Figure 4

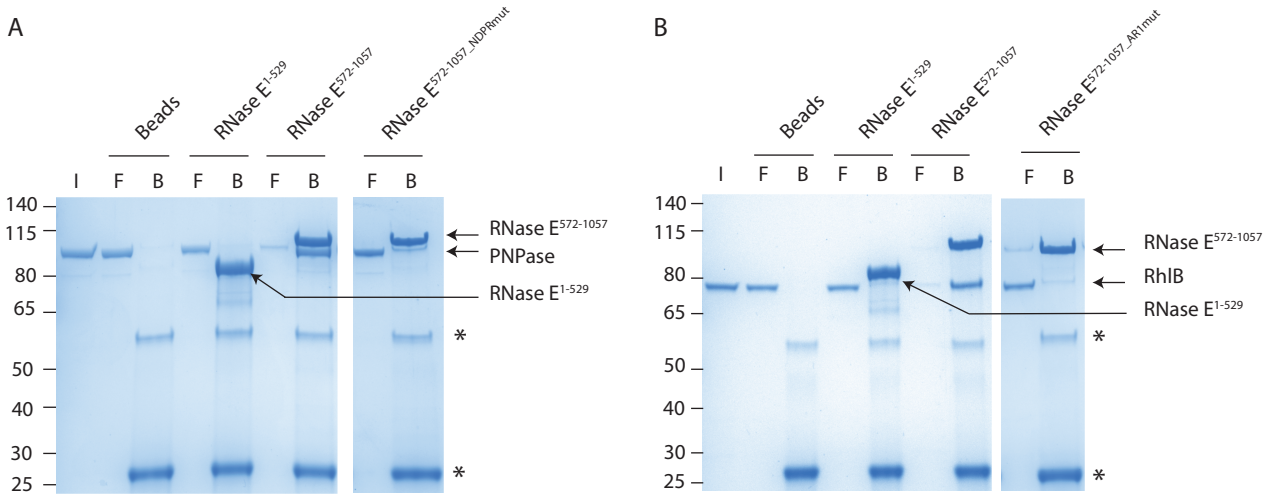
A
Beads
RNase E1-529
RNase E572-1057
RNase E572-1057_NDPRmut
I F B F B F B F B
140
115
80
65
50
40
30
25
RNase E572-1057
PNPase
RNase E1-529
*
*
B
Beads
RNase E1-529
RNase E572-1057
RNase E572-1057_AR1mut
I F B F B F B F B
140
115
80
65
50
40
30
25
RNase E572-1057
RhlB
RNase E1-529
*
*

Figure 5

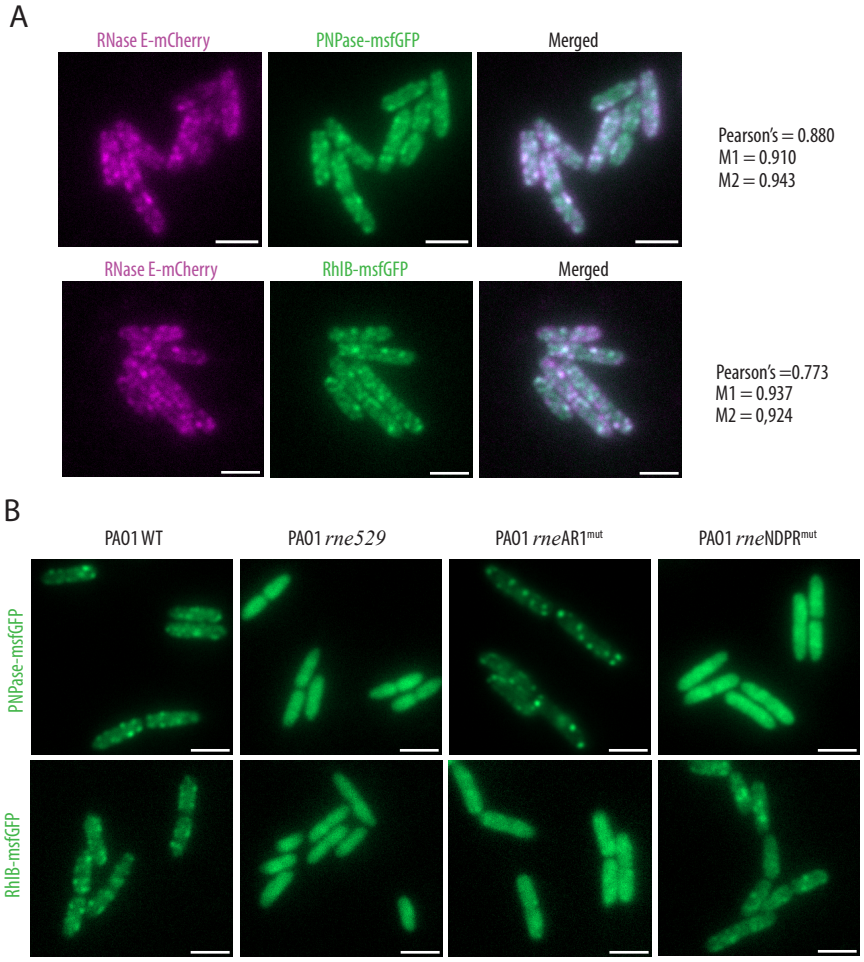
A
RNase E-mCherry
PNPase-msfGFP
Merged
Pearson's = 0.880
M1 = 0.910
M2 = 0.943
RNase E-mCherry
RhlB-msfGFP
Merged
Pearson's =0.773
M1 = 0.937
M2 = 0,924
B
PAO1 WT
PAO1 rne529
PAO1 rneAR1mut
PAO1 rneNDPRmut
PNPase-msfGFP
RhlB-msfGFP

Figure 6

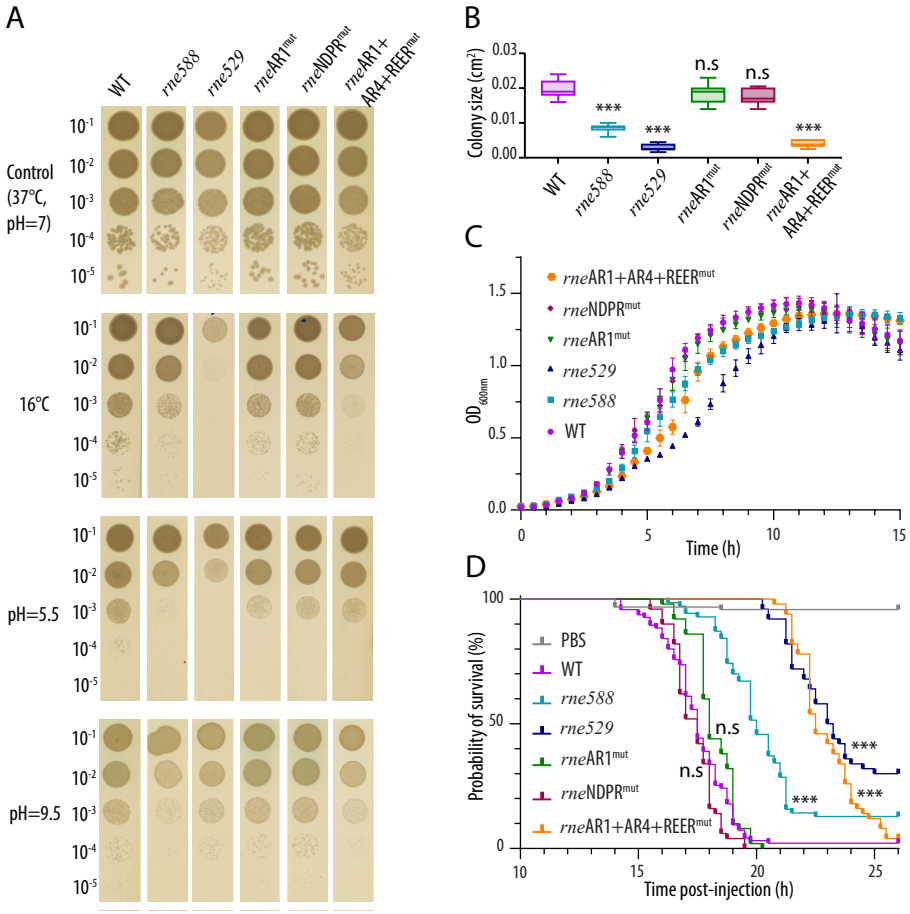
A
WT
rne588
rne529
rneAR1mut
rneNDPRmut
rneAR1+ AR4+REERmut
Control (37°C, pH=7)
16°C
pH=5.5
pH=9.5
B
Colony size (cm²)
n.s
***
C
rneAR1+AR4+REERmut
rneNDPRmut
rneAR1mut
rne529
rne588
WT
OD600nm
Time (h)
D
PBS
WT
rne588
rne529
rneAR1mut
rneNDPRmut
rneAR1+AR4+REERmut
Probability of survival (%)
Time post-injection (h)

Figure 7

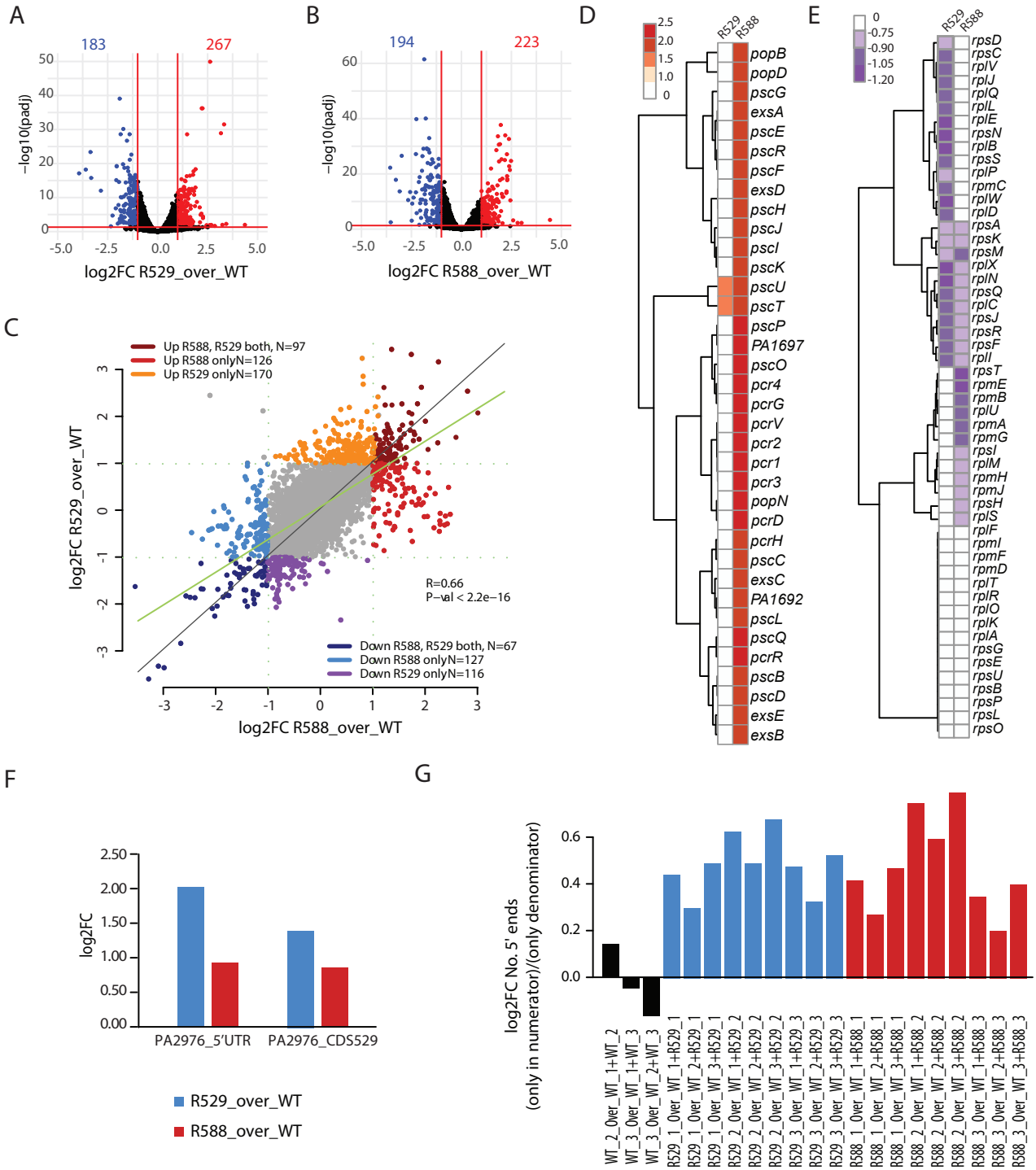
A
183
267
−log10(padj)
log2FC R529_over_WT
B
194
223
−log10(padj)
log2FC R588_over_WT
C
Up R588, R529 both, N=97
Up R588 onlyN=126
Up R529 onlyN=170
Down R588, R529 both, N=67
Down R588 onlyN=127
Down R529 onlyN=116
R=0.66
P−val < 2.2e−16
log2FC R529_over_WT
log2FC R588_over_WT
D
R529
R588
popB
popD
pscG
exsA
pscE
pscR
pscF
exsD
pscH
pscJ
pscI
pscK
pscU
pscT
pscP
PA1697
pscO
pcr4
pcrG
pcrV
pcr2
pcr1
pcr3
popN
pcrD
pcrH
pscC
exsC
PA1692
pscL
pscQ
pcrR
pscB
pscD
exsE
exsB
E
R529
R588
rpsD
rpsC
rplV
rplJ
rplQ
rplL
rplE
rpsN
rplB
rpsS
rplP
rpmC
rplW
rplD
rpsA
rpsK
rpsM
rplX
rplN
rpsQ
rplC
rpsJ
rpsR
rpsF
rplI
rpsT
rpmE
rpmB
rplU
rpmA
rpmG
rpsI
rplM
rpmH
rpmJ
rpsH
rplS
rplF
rpmI
rpmF
rpmD
rplT
rplR
rplO
rplK
rplA
rpsG
rpsE
rpsU
rpsB
rpsP
rpsL
rpsO
F
log2FC
PA2976_5'UTR
PA2976_CDS529
R529_over_WT
R588_over_WT
G
log2FC No. 5' ends
(only in numerator)/(only denominator)
WT_2_Over_WT_1+WT_2
WT_3_Over_WT_1+WT_3
WT_3_Over_WT_2+WT_3
R529_1_Over_WT_1+R529_1
R529_1_Over_WT_2+R529_1
R529_1_Over_WT_3+R529_1
R529_2_Over_WT_1+R529_2
R529_2_Over_WT_2+R529_2
R529_2_Over_WT_3+R529_2
R529_3_Over_WT_1+R529_3
R529_3_Over_WT_2+R529_3
R529_3_Over_WT_3+R529_3
R588_1_Over_WT_1+R588_1
R588_1_Over_WT_2+R588_1
R588_1_Over_WT_3+R588_1
R588_2_Over_WT_1+R588_2
R588_2_Over_WT_2+R588_2
R588_2_Over_WT_3+R588_2
R588_3_Over_WT_1+R588_3
R588_3_Over_WT_2+R588_3
R588_3_Over_WT_3+R588_3

Figure 8

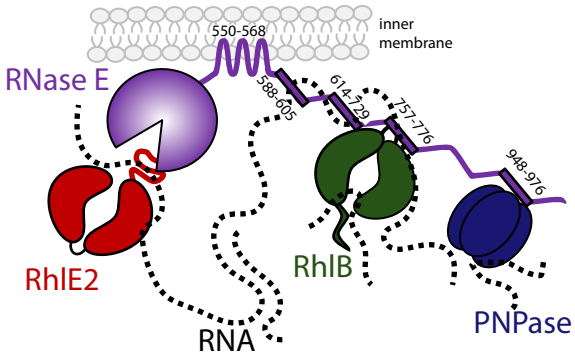
inner
membrane
550-568
RNase E
588-605
614-729
757-776
948-976
RhlE2
RhlB
PNPase
RNA